Cretaceous provenance change in the Hegang Basin and its connection with the Songliao Basin, NE China: evidence for lithospheric extension driven by palaeo-Pacific roll-back

MINGDAO SUN[1,2,3], HANLIN CHEN[1]*, FENGQI ZHANG[1], SIMON A. WILDE[2], A MINNA[1], XIUBIN LIN[1] & SHUFENG YANG[1]

[1]*Department of Earth Science, Zhejiang University, Hangzhou, Zhejiang 310027, China*

[2]*Department of Applied Geology, Curtin University, Perth, WA 6845, Australia*

[3]*Guangzhou Institute of Geochemistry, Chinese Academy of Sciences, Guangzhou 510640, China*

**Corresponding author (e-mail: hlchen@zju.edu.cn)*

Abstract: The Cretaceous Hegang Basin is located on the Jiamusi Block, NE China, and separated from the Songliao Basin by the Lesser Xing'an Range (LXR). Seismic interpretation shows that the Chengzihe, Muling and Dongshan formations of the Hegang Basin thicken eastwards with westwards onlap, indicating that the LXR existed as a palaeo-uplift during that period, whereas the Houshigou Formation shows no thickness change, indicating that the LXR was possibly under water at this time. This is supported by results of detrital zircon analysis from the Hegang Basin in which the Chengzihe Formation is dominated by approximately 180 Ma zircons, which can only be provided by the LXR, whereas the Houshigou Formation records no early Jurassic ages. This view is consistent with previous studies of the Songliao Basin for a provenance change between the Denglouku and Quantou formations. We conclude that the LXR was a highland during deposition of the Chengzihe, Muling and Dongshan formations but that it was under water when the Houshigou Formation was deposited. There was thus a connection between the Hegang and Songliao basins, which marks an eastwards migration of the depositional and extensional centre of the Songliao–Hegang basin system. This eastwards migration implies lithospheric extension driven by palaeo-Pacific roll-back.

Zircon grains in clastic sedimentary rocks are derived from the weathering of the surrounding source rocks, and are recognized as being highly resistant to chemical and physical weathering and other sedimentary processes (Jackson & Sherman 1953). Detrital zircon analysis is widely recognized as a powerful tool for interpreting the provenance of sedimentary rocks (Drewery *et al.* 1987; Thomas 2011) because it has the ability to link sedimentary basins to their surrounding source regions (Riggs *et al.* 1996). Detrital zircon analysis can also be applied to infer maximum depositional ages of strata (Dickinson & Gehrels 2009), to reconstruct supercontinent cycles (Li *et al.* 1995) and to reflect the tectonic settings of the basins in which they were deposited (Cawood *et al.* 2012).

The Hegang Basin is located to the east of the Lesser Xing'an Range (LXR), the Zhangguangcai Range (ZR) and the Songliao Basin, and lies within the Jiamusi Block to the west of the Sanjiang Basin, NE China (Fig. 1). It is 100 km long from north to south, and 28 km wide from east to west, with a total area of approximately 2800 km^2. The Hegang Basin has been mined for coal since 1917 and contained China's largest opencast coal mine (before 2010) – the Lingbei Opencast Mine, which is now part of the Hegang National Mine Park. The coal types are mainly bituminous coal to anthracite. The strata of the Hegang Basin were previously considered to be Late Jurassic in age; however, a recent study based on palaeontology suggests that they were deposited in the Early Cretaceous (Sha *et al.* 2002).

The Songliao Basin is located between the LXR and ZR to the east, and the Great Xing'an Range to the west (Fig. 1). It is approximately 1000 km long from north to south, and 400 km wide from east to west, with a total area of approximately 350 000 km^2. The Songliao Basin contains oil- and gas-bearing non-marine sedimentary strata, and is one of the largest oil fields in China. It includes the Daqing oil field, which started production in 1959. The structure and sedimentology of the Songliao Basin have been well studied because of extensive oil and gas exploration and development (Wu *et al.* 2007; Feng *et al.* 2010*b*, 2011). Its structural evolution has been subdivided into three stages: synrift stage (the Huoshiling,

From: Gibson, G. M., Roure, F. & Manatschal, G. (eds) *Sedimentary Basins and Crustal Processes at Continental Margins: From Modern Hyper-extended Margins to Deformed Ancient Analogues.* Geological Society, London, Special Publications, **413**, http://dx.doi.org/10.1144/SP413.2

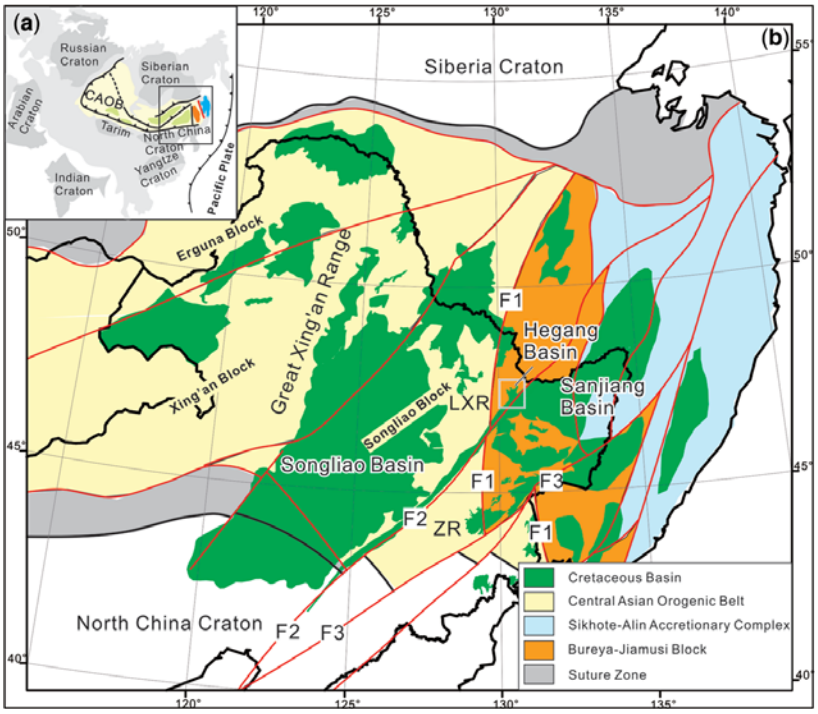

Fig. 1. (**a**) Location of the Central Asian Orogenic Belt (CAOB) and adjacent cratons. (**b**) Basin distribution in NE China and adjacent areas (after Zhou *et al.* 2009; Sorokin *et al.* 2010; Wu *et al.* 2011): F1, Mudanjiang Fault; F2, Yi-Shu Fault; F3, Dun-Mi Fault; LXR, Lesser Xing'an Range; ZR, Zhangguangcai Range.

Shahezi, Yingcheng and Denglouku formations) with asthenospheric upwelling and crustal extension; post-rift stage (the Quantou, Qingshankou, Yaojia and Nenjiang formations) with lithosphere cooling and subsidence; and the structural inversion stage (the Sifangtai, Mingshui, Yi'an, Da'an and Taikang formations) with compression and folding (Ren *et al.* 2002; Feng *et al.* 2010*a*).

Along the present eastern boundary of the Songliao Basin, most of the post-rift strata are deep lake facies (Zhang & Bao 2009; Feng *et al.* 2010*a*, 2013; Gao *et al.* 2010; Xi *et al.* 2011; Wang *et al.* 2013). This poses some important scientific questions.

- Where was the original eastern boundary of the Songliao Basin in the post-rift period?
- Did the Songliao Basin ever spread east over the LXR?
- What is the relationship between the Songliao and Hegang basins?

In this study, we report a sensitive high-resolution ion microprobe (SHRIMP) zircon U–Pb age of a tuff from the Houshigou Formation, and detrital zircon ages for the Chengzihe and Houshigou formations of the Hegang Basin. In light of these results, we review the distribution of Late Triassic–Early Jurassic igneous rocks in NE China and the detrital zircon geochronology of the Songliao Basin in order to test for any similarities with the Hegang Basin. This study will help in understanding sedimentary basin development and the tectonic evolution of East Asia. It is also relevant to the timing of changes in tectonic regime, associated with the advance and retreat of the palaeo-Pacific Plate, which has dominated the architecture of eastern China since the early Mesozoic.

Geological setting

NE China and adjacent regions in Far East Russia are made up of several massifs and terranes that are located between the Siberia and North China cratons (Fig. 1), including the Erguna, Xing'an, Songliao, Bureya and Jiamusi blocks, and the Sikhote–Alin accretionary complex (Wu *et al.* 2005; Yu *et al.* 2008; Kotov *et al.* 2009; Sorokin *et al.* 2010; Zhou *et al.* 2011*a*). The Erguna, Xing'an and Songliao blocks are considered to be the eastern part of the Central Asian Orogenic Belt (CAOB) that amalgamated in the Palaeozoic (Xiao *et al.* 2009, 2010), whereas the Jiamusi block and Sikhote–Alin accretionary complex are early Mesozoic circum-Pacific accreted terranes (Zhou *et al.* 2009; Wu *et al.* 2011). The amalgamated

Erguna, Xing'an and Songliao blocks collided with the North China Craton in the Permian (Xiao *et al.* 2003), and with the Siberia Craton in the late Palaeozoic–early Mesozoic (Kravchinsky *et al.* 2002). Final collision with the Jiamusi Block occurred in the early Mesozoic (Zhou *et al.* 2009), forming the unified Jiamusi–Mongolia block (Wang *et al.* 2011). The ocean separating the Jiamusi–Mongolia block from the Siberia Craton closed completely in the early Early Cretaceous (Cogne *et al.* 2005).

The Songliao Block is overlain by Mesozoic–Cenozoic strata of the Songliao Basin. Most of the basement beneath the Songliao Basin is composed of Palaeozoic–Mesozoic granitoids and Palaeozoic strata (Wu *et al.* 2000, 2001; Gao *et al.* 2007; Pei *et al.* 2007; Yu *et al.* 2008; Zhou *et al.* 2012), with minor Proterozoic granitoids (Wang *et al.* 2006). In the eastern part of the Songliao Block, the basement was uplifted and forms the LXR and ZR, which also contain Palaeozoic–Mesozoic granitoids and Palaeozoic strata (Meng *et al.* 2010, 2011; Wang *et al.* 2012*a*, *b*).

The Jiamusi Block has a pre-Mesozoic basement that is composed mainly of the Mashan Complex, the Heilongjiang Complex and Permian granite (Wu *et al.* 2011). The Mashan Complex makes up the main part of the Jiamusi Block and consists of khondalitic rocks with a metamorphic age of 500 Ma (Wilde *et al.* 1999, 2000, 2003). The Heilongjiang Complex is distributed in the western part of the Jiamusi Block, and consists of ultramafic rocks, blueschist-facies pillow basalts, carbonates and mylonitic mica schists, which are considered to represent a mélange along the suture between the Jiamusi and Songliao blocks (Wu *et al.* 2007; Zhou *et al.* 2009).

Stratigraphy and structure of the Hegang Basin

Stratigraphy

The basement of the Hegang Basin is composed of the Mashan and Heilongjiang complexes and Jurassic granites (Fig. 2). The basin strata are named, from bottom to top, the Chengzihe, Muling, Dongshan, Houshigou and Songmuhe formations (Figs 2 & 3). The Chengzihe, Muling and Dongshan formations constitute the Jixi Group (Gu *et al.* 1997;

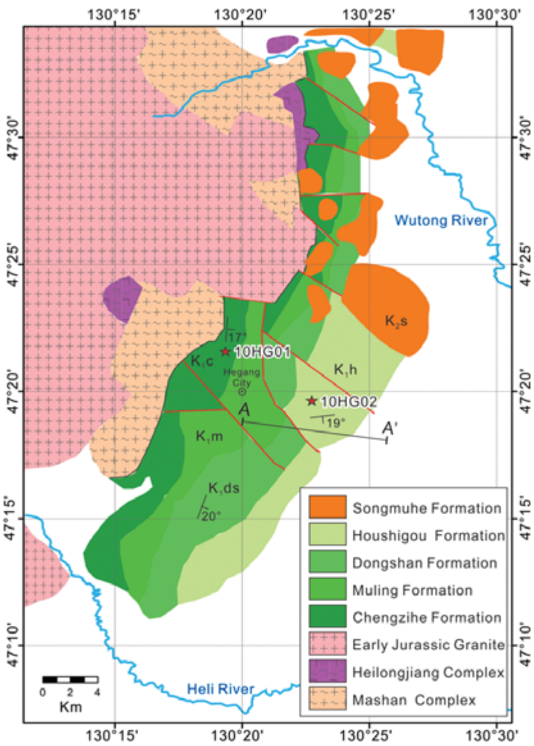

Fig. 2. Simplified geological map of the Hegang Basin, based on the Hegang and Jiamusi 1:200 000 geological maps.

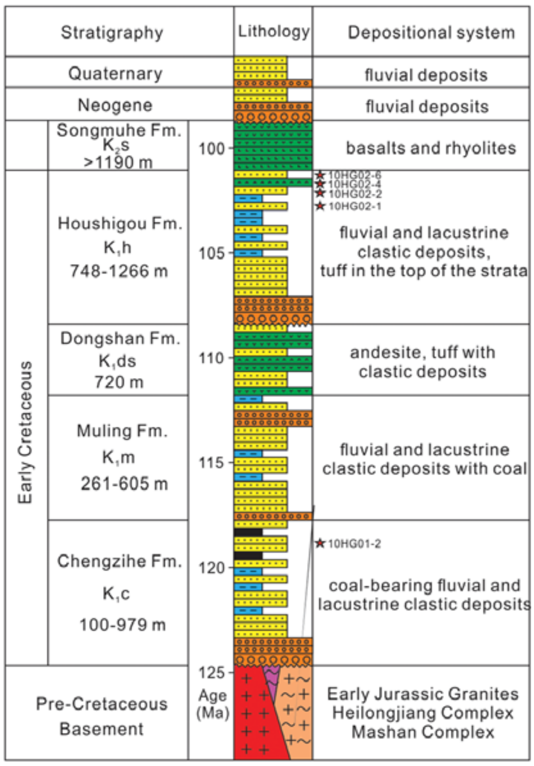

Fig. 3. Stratigraphic column of the Hegang Basin showing the relative positions of samples, based on the Hegang and Jiamusi 1:200 000 geological maps; the stars show the relative location of samples used in this study.

Li *et al.* 2006), and their contacts are conformable (Sha *et al.* 2002, 2003, 2009; Sha 2007).

The Chengzihe Formation (K_1c) ranges in thickness from 100 to 979 m. The lower part consists of fluvial facies with medium- to coarse-grained sandstone, conglomerate, siltstone, mudstone and tuff. The middle part consists of fluvial and lacustrine facies fine- to medium-grained sandstone, siltstone and mudstone, with minor coarse sandstone and conglomerate. The middle unit contains 36 coal seams of mineable quality and is also rich in plant fossils. The upper part of the Chengzihe Formation consists of fluvial facies, fine-grained sandstone and siltstone, with mudstone and tuff.

The Muling Formation (K_1m) conformably overlies the Chengzihe Formation, with a thickness ranging from 261 to 605 m. It consists of thick yellowish-brown conglomerate, grey sandstone, and dark grey siltstone and mudstone, with thin layers of tuff, indicating fluvial to deltaic facies with occasional distal volcanism.

The Dongshan Formation (K_1ds) consists of grey-green andesite, andesitic agglomerate, volcanic breccia and tuff, with some siltstone and sandstone. Its total thickness is 720 m.

The Houshigou Formation (K_1h) overlies the Dongshan Formation with a minor angular unconformity, and it ranges in thickness from 748 to 1266 m. The lower part consists of fluvial facies conglomerate and yellow sandstone. The clasts in the conglomerate consist mainly of andesite, gneiss and granite. The upper part of the Houshigou Formation consists of lacustrine facies black, fine-grained sandstone, siltstone and mudstone, with a tuff interlayer at the top.

The Songmuhe Formation (K_2s) consists of volcanic rocks with thickness of 1087 m. It has two members. The lower part, the Xigemu Member, consists of andesite, basalt and tuff, with a total thickness of 600 m. The upper part, the Aoqi Member, consists of rhyolite, tuff and volcanic breccia, with a total thickness of 487 m.

Structure

The Early Cretaceous Hegang Basin was possibly part of the Sanjiang Basin (Fig. 1), as suggested by Zhang *et al.* (2012). However, the structural prototype of the Hegang Basin was difficult to rebuild because it is separated from the Sanjiang Basin by the Cenozoic Yishu Fault (F2, Fig. 1) and was also destroyed by a westwards Late Cretaceous–Cenozoic thrust fault (Huang *et al.* 2003; Sun *et al.* 2006), as also shown in the seismic profile (Fig. 4). Nevertheless, the seismic profile still provides important information that helps in the understanding of the provenance of the Hegang Basin. In general, the Early Cretaceous strata dip eastwards at approximately 15°, showing a monoclinal structure. In detail, the Chengzihe, Muling and Dongshan formations thicken eastwards with westwards onlap on to the early Mesozoic granite basement, which is the main component of LXR, indicating that the LXR existed as a palaeo-uplift during that period, while the Houshigou Formation has no change in thickness, indicating that the LXR was possibly under water at this time. Hence, the structure of the Hegang Basin implies a possible provenance change from the Chengzihe Formation to the Houshigou Formation.

Sample locations and petrology

Two sections were chosen for this investigation, both located close to Hegang City in eastern Heilongjiang Province, in order to sample and compare the rocks from the Chengzihe and Houshigou formations, which are located beneath and above the major unconformity surface, respectively.

Section 10HG01 (Fig. 5) is in the Lingbei Coal Mine, where sandstone sample 10HG01-2 was collected (47°21′30″N, 130°19′0″E) from the middle part of the Chengzihe Formation. This section is rich in plant fossils characterized by Filicopsida, and several species of Ginkgopsida and Coniferopsida (Fig. 5). Sun & Dilcher (2002) and Liu (2006) gave a statistical analysis of 40% Filicophytina, 20% Bennettitales, 10% *Ginkgo*, 10% Coniferopsida and 10% early angiosperms. These authors correlate this assemblage with the Barremian Stage. It further indicates that the climate of the Jiamusi area at this time was warm and humid, possibly even subtropical.

Section 10HG02 (Fig. 6) is at a location (47°19′39″N, 130°22′44″E) near fishponds outside of Wugongli Village, on the western side of the Haluo Highway. Samples 10HG02-1, 10HG02-2, 10HG02-4 and 10HG02-6 were collected from the upper part of the Houghigou Formation. Sample 10HG01-2 is a grey-white coarse-grained sandstone. The grains are 0.3–1 mm in diameter, subangular and poorly sorted, and are composed of 50% quartz, 30% feldspar and 20% lithic fragments. The accessory minerals are mainly zircon, pyrite and siderite. Samples 10HG02-1 and 10HG02-2 are yellow–dark yellow fine-grained sandstone. The grains are mostly 0.1–0.3 mm in diameter, angular and moderately well sorted, and composed approximately of 60% quartz, 30% feldspar and 10% lithic fragments. The accessory minerals are mainly garnet and titanite. Sample 10HG02-4 is a white rhyolitic tuff with crystal and glass fragments. Sample 10HG02-6 is a yellow coarse-grained sandstone, composed of 70% quartz, 20% feldspar and 5% lithic fragments.

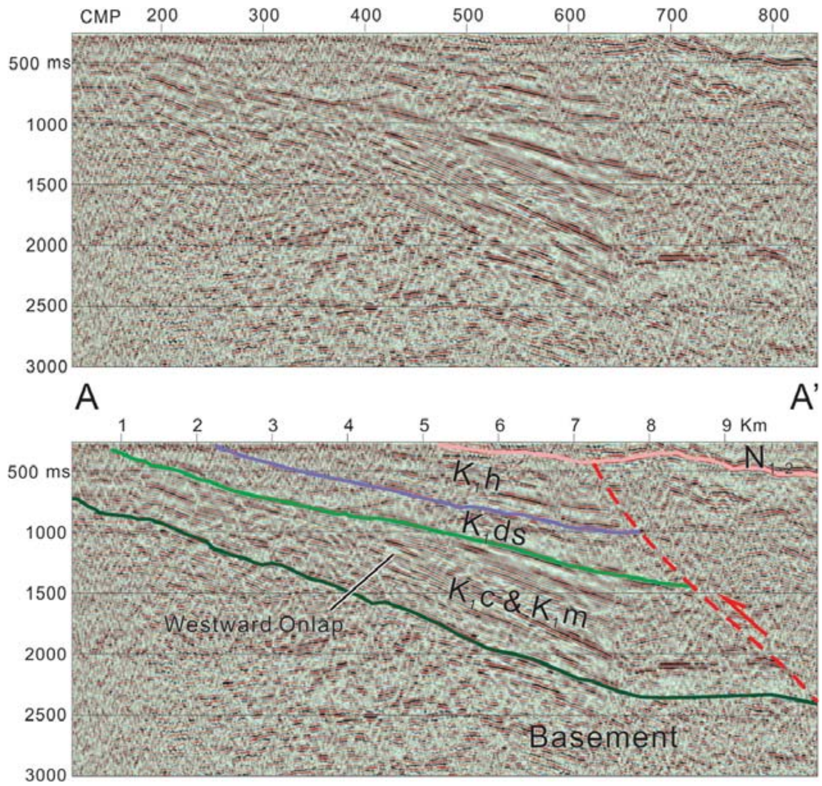

Fig. 4. Seismic profile across the Hegang Basin with an interpretation showing that the Chengzihe and Muling formations thicken from west to east with a westwards onlap on to the basement. Seismic data were provided by PetroChina.

Analytical methods

Approximately 3 kg samples were collected from each site for zircon separation. Zircon crystals were extracted by crushing, and by heavy liquid and magnetic separation at the Langfang Geological Services Corporation, Hebei Province, China. More than 2000 zircon grains were extracted from each sample. Zircons from the tuff sample HG02-4, taken to the Beijing SHRIMP Centre, were mounted

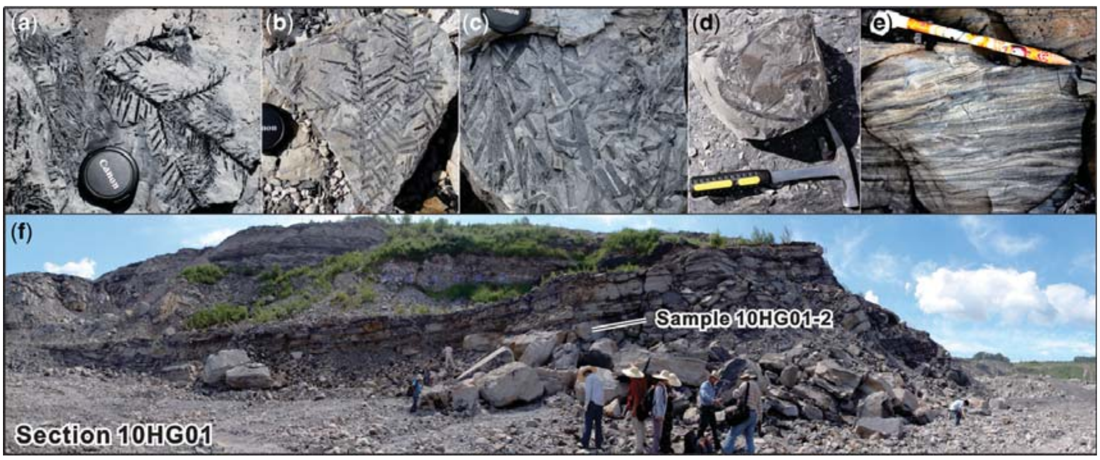

Fig. 5. Photograph of section 10HG01, Chengzihe Formation: (**a**) & (**b**) Filicophytina; (**c**) Bennettitales; (**d**) Ginkgo leaf; (**e**) laminae in siltstone; and (**f**) photograph showing the sample location.

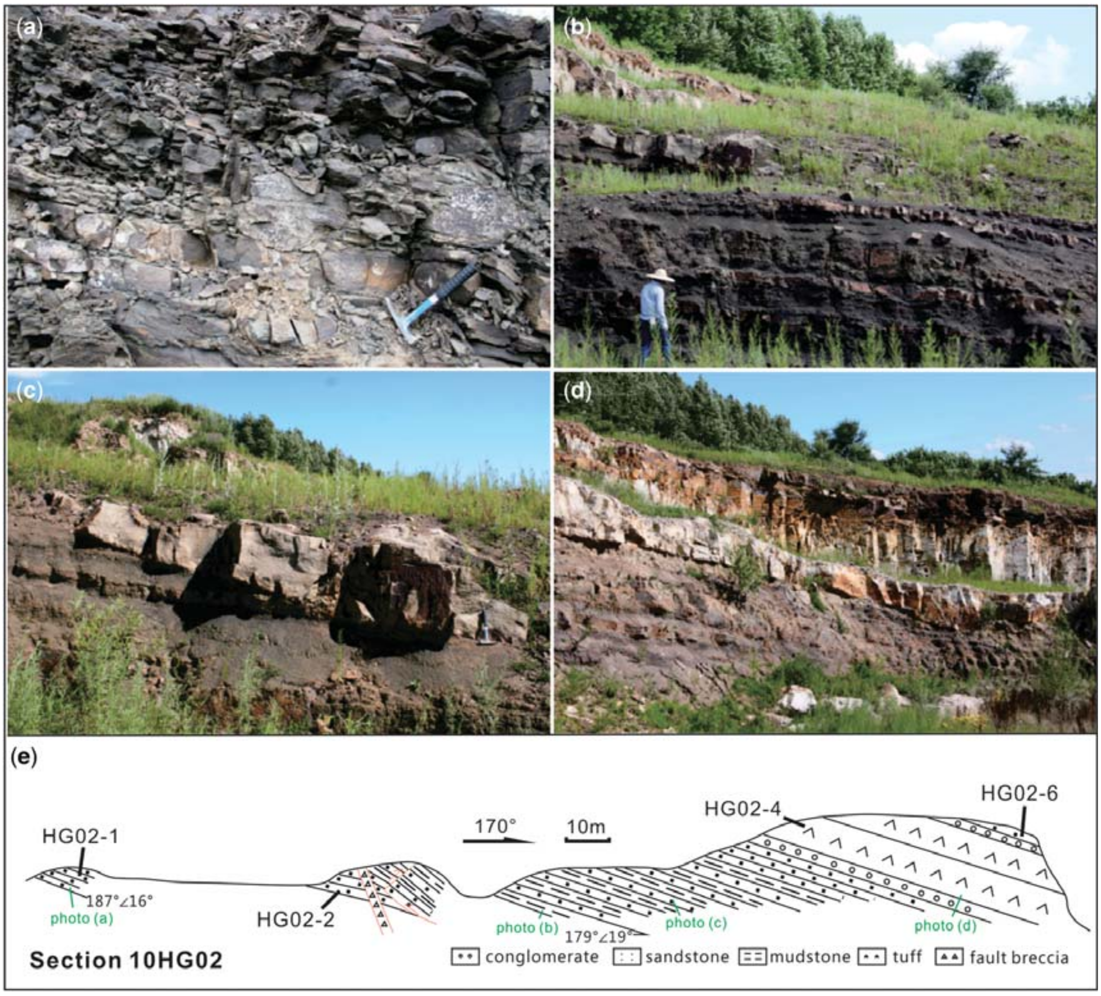

Fig. 6. Photograph of section 10HG02, Houshigou Formation: (**a**) black siltstone; (**b**) thin layered grey-yellow sandstone with a dark mudstone interbed; (**c**) small channel sandbody; (**d**) white tuff; and (**e**) section sketch, showing the sample sites.

along with the TEMORA standard (Black *et al.* 2003) and polished to reveal the grain centres. Zircons from the sandstones, taken to the Second Institute of Oceanography of State Oceanic Administration of China in Hangzhou, were also mounted and polished. Cathodoluminescence (CL) images were taken using a Philips XL30 scanning electron microscope at Curtin University, Perth following U–Pb analysis. Most zircons from each sample are transparent, pale yellow and euhedral prismatic, and are typically magmatic with concentric oscillatory zonation evident in the CL images (Fig. 7).

SHRIMP U–Pb dating was performed using a SHRIMP II ion microprobe at the Beijing SHRIMP Centre following standard procedures (Wan *et al.* 2005). The mass resolution was approximately 5000 at 1% peak height. The spot size of the ion beam was 25–30 μm, and five scans through the mass range were used for data collection. Standard SL13 (572 Ma, U = 238 ppm) was used for U concentration and age calibration, and TEMORA (417 Ma) (Black *et al.* 2003) was used to monitor analytical conditions. Ages and Concordia diagrams were calculated using the programs Squid 1.03 (Ludwig 2001) and Isoplot 3.0 (Ludwig 2003).

Laser ablation inductively coupled plasma mass spectrometry (LA-ICP-MS) U–Pb dating was carried out at the State Key Laboratory of Mineral Deposits Research at Nanjing University. The LA-ICP-MS consisted of an Agilent 7500 s ICP-MS attached to a Merchantek/NWR 213 nm laser ablation system. The diameter of the analysis spot was 25 μm. The repetition rate and power was 5 Hz and 68%, respectively. About 100 grains of each

Fig. 7. CL images for representative zircons from the sandstones of the Chengzihe and Houshigou formations.

sandstone sample were analysed. U–Pb fractionation was corrected using standard zircon GJ ($^{207}Pb/^{206}Pb$ age of 608.5 ± 1.5 Ma: Jackson *et al.* 2004), and reproducibility was controlled using a standard zircon Mud Tank (MT) ($^{207}Pb/^{206}Pb$ age of 732 ± 5 Ma: Black & Gulson 1978). The analytical data were processed using Glitter 4.4 software. Because ^{204}Pb could not be measured owing to a low signal and interference from ^{204}Hg in the gas supply, the common lead correction was carried out using the Excel program ComPbcorr#3-15G (Andersen 2002). The Concordia diagrams and histograms were plotted using Isoplot 3.0 (Ludwig 2003). In this investigation, zircons younger than 1.0 Ga were calculated using the $^{206}Pb/^{238}U$ age, whereas older ones were calculated using the $^{207}Pb/^{206}Pb$ age.

Analytical results

Sample 10HG01-2

Sample 10HG01-2, collected from the Chengzihe Formation, contained zircon grains 40–400 μm long and a total of 109 randomly selected grains were analysed (Table 1). Two grains were excluded from the calculations because of discordance. The remaining 107 grains were concordant at the 90% confidence level. The $^{206}Pb/^{238}U$ ages fall mainly into three groups (Fig. 8a): 203–153 Ma (44%), 285–207 Ma (41%) and 492–427 Ma (9%), with peaks at approximately 180, 250 and 450 Ma (Fig. 8b). The age of 122 ± 2 Ma for the youngest grain defines the maximum depositional age of the Chengzihe Formation.

Sample 10HG02-1

Sample 10HG02-1 was collected from the Houshigou Formation. Zircon grains were 40–200 μm long and a total of 84 randomly selected grains were analysed (Table 2). One grain was excluded from the calculations because of the large error. The remaining 83 grains gave concordant ages at the 90% confidence level. The $^{206}Pb/^{238}U$ ages of Phanerozoic zircons mainly fall into three populations (Fig. 8c): 283–223 Ma (39%), 484–427 Ma (14%) and 522–501 Ma (14%), with peaks at approximately 250, 450 and 510 Ma, respectively (Fig. 8d). The youngest zircon has an age of 104 ± 2 Ma, thus constraining the maximum age of deposition. There is also 12% of Precambrian zircons in the population, with $^{207}Pb/^{206}Pb$ ages ranging from 1.4 to 0.6 Ga.

Table 1. *LA-ICP-MS U–Pb results for detrital zircons from sample 10HG01-2, Chengzihe Formation of the Hegang Basin*

Spots	Element (ppm)		Th/U	Corrected isotopic ratios						Corrected ages (Ma)					
	Th	U		$^{207}Pb/^{206}Pb$	1σ	$^{207}Pb/^{235}U$	1σ	$^{206}Pb/^{238}U$	1σ	$^{207}Pb/^{206}Pb$	1σ	$^{207}Pb/^{235}U$	1σ	$^{206}Pb/^{238}U$	1σ
HG01-01	81	97	0.84	0.0495	0.0016	0.1890	0.0061	0.0277	0.0004	172	47	176	5	176	3
HG01-02	32	370	0.09	0.0593	0.0009	0.7508	0.0124	0.0918	0.0012	579	17	569	7	566	7
HG01-03	242	373	0.65	0.0501	0.0009	0.2178	0.0043	0.0315	0.0004	200	23	200	4	200	3
HG01-04	153	224	0.68	0.0518	0.0020	0.1988	0.0075	0.0279	0.0005	276	55	184	6	177	3
HG01-05	7	15	0.45	0.0563	0.0026	0.5839	0.0266	0.0753	0.0013	462	69	467	17	468	8
HG01-06	242	116	2.09	0.0495	0.0025	0.1793	0.0089	0.0263	0.0005	173	79	167	8	167	3
HG01-07	110	225	0.49	0.0505	0.0014	0.2318	0.0062	0.0333	0.0005	218	36	212	5	211	3
HG01-08	54	111	0.49	0.0577	0.0010	0.6215	0.0117	0.0782	0.0011	517	20	491	7	485	6
HG01-09	280	339	0.83	0.0497	0.0009	0.2001	0.0038	0.0292	0.0004	182	22	185	3	185	2
HG01-10	323	630	0.51	0.0499	0.0009	0.2014	0.0037	0.0293	0.0004	191	20	186	3	186	2
HG01-11	159	366	0.43	0.0498	0.0008	0.2109	0.0038	0.0307	0.0004	187	20	194	3	195	3
HG01-12	162	156	1.04	0.0511	0.0011	0.2700	0.0059	0.0383	0.0005	245	26	243	5	242	3
HG01-13	77	61	1.27	0.0495	0.0031	0.1820	0.0110	0.0267	0.0006	169	100	170	9	170	3
HG01-14	164	506	0.32	0.0515	0.0007	0.2870	0.0046	0.0404	0.0005	264	17	256	4	255	3
HG01-15	236	301	0.78	0.0512	0.0009	0.2768	0.0050	0.0392	0.0005	248	20	248	4	248	3
HG01-16	253	205	1.23	0.0520	0.0011	0.3123	0.0066	0.0435	0.0006	287	25	276	5	275	4
HG01-17	130	200	0.65	0.0501	0.0012	0.2151	0.0051	0.0311	0.0004	201	30	198	4	198	3
HG01-18	125	126	0.99	0.0498	0.0015	0.1931	0.0059	0.0281	0.0004	184	43	179	5	179	3
HG01-19	264	273	0.97	0.0495	0.0010	0.2260	0.0045	0.0331	0.0005	171	23	207	4	210	3
HG01-20	186	411	0.45	0.0504	0.0009	0.2343	0.0043	0.0337	0.0005	213	20	214	3	214	3
HG01-21	614	639	0.96	0.0557	0.0007	0.5397	0.0078	0.0703	0.0009	439	14	438	5	438	5
HG01-22	440	766	0.58	0.0500	0.0008	0.2074	0.0037	0.0301	0.0004	195	20	191	3	191	3
HG01-23	111	152	0.73	0.0503	0.0013	0.2263	0.0057	0.0327	0.0005	207	33	207	5	207	3
HG01-24	326	741	0.44	0.0502	0.0007	0.2268	0.0036	0.0328	0.0004	202	16	208	3	208	3
HG01-25	186	240	0.78	0.0505	0.0010	0.2189	0.0044	0.0314	0.0004	219	24	201	4	199	3
HG01-26	39	93	0.42	0.0520	0.0021	0.2735	0.0106	0.0381	0.0007	285	58	245	8	241	4
HG01-27	251	567	0.44	0.0515	0.0007	0.2954	0.0044	0.0416	0.0005	264	16	263	3	263	3
HG01-28	500	379	1.32	0.0497	0.0009	0.1899	0.0035	0.0277	0.0004	181	21	177	3	176	2
HG01-30	119	206	0.58	0.0506	0.0011	0.2320	0.0049	0.0333	0.0005	223	25	212	4	211	3
HG01-31	69	90	0.77	0.0529	0.0016	0.2260	0.0067	0.0310	0.0005	322	40	207	6	197	3
HG01-32	420	308	1.36	0.0491	0.0014	0.1661	0.0047	0.0245	0.0004	155	39	156	4	156	2
HG01-33	303	463	0.65	0.0570	0.0007	0.6229	0.0086	0.0793	0.0010	491	14	492	5	492	6
HG01-34	99	136	0.73	0.0505	0.0013	0.2460	0.0062	0.0353	0.0005	219	33	223	5	224	3
HG01-35	117	115	1.02	0.0517	0.0012	0.2715	0.0062	0.0381	0.0005	271	28	244	5	241	3
HG01-36	71	67	1.06	0.0517	0.0018	0.2814	0.0096	0.0395	0.0006	273	50	252	8	250	4
HG01-29	99	89	1.11	0.0528	0.0012	0.2898	0.0067	0.0398	0.0006	321	29	258	5	252	3
HG01-37	232	468	0.50	0.0519	0.0009	0.2197	0.0041	0.0307	0.0004	280	21	202	3	195	3

HG01-39	333	540	0.62	0.0561	0.0007	0.5746	0.0080	0.0742	0.0009	458	14	461	5	462	6
HG01-40	196	402	0.49	0.0508	0.0009	0.2472	0.0046	0.0353	0.0005	229	21	224	4	224	3
HG01-41	358	749	0.48	0.0502	0.0007	0.2215	0.0035	0.0320	0.0004	203	17	203	3	203	2
HG01-42	550	682	0.81	0.0521	0.0012	0.2089	0.0049	0.0291	0.0004	290	30	193	4	185	3
HG01-43	301	382	0.79	0.0513	0.0009	0.1919	0.0036	0.0271	0.0004	255	22	178	3	173	2
HG01-44	144	303	0.47	0.0500	0.0011	0.2054	0.0045	0.0298	0.0004	196	27	190	4	189	3
HG01-45	142	136	1.05	0.0497	0.0017	0.1804	0.0061	0.0263	0.0004	180	49	168	5	168	3
HG01-46	206	333	0.62	0.0521	0.0014	0.1754	0.0046	0.0244	0.0004	289	34	164	4	156	2
HG01-47	526	839	0.63	0.0515	0.0008	0.2163	0.0034	0.0305	0.0004	262	17	199	3	193	2
HG01-48	925	728	1.27	0.0515	0.0012	0.2006	0.0046	0.0283	0.0004	263	28	186	4	180	2
HG01-38	115	68	1.68	0.0495	0.0020	0.1861	0.0071	0.0273	0.0005	173	58	173	6	173	3
HG01-49	287	375	0.77	0.0496	0.0009	0.1889	0.0035	0.0276	0.0004	177	21	176	3	176	2
HG01-50	50	65	0.76	0.0548	0.0018	0.2611	0.0084	0.0346	0.0005	402	44	236	7	219	3
HG01-51	197	494	0.40	0.0498	0.0011	0.1935	0.0041	0.0282	0.0004	188	26	180	4	179	2
HG01-52	226	323	0.70	0.0490	0.0012	0.1650	0.0039	0.0244	0.0003	148	31	155	3	156	2
HG01-53	191	446	0.43	0.0500	0.0008	0.2164	0.0035	0.0314	0.0004	196	17	199	3	199	2
HG01-54	131	167	0.78	0.0493	0.0018	0.1752	0.0062	0.0258	0.0004	161	52	164	5	164	3
HG01-55	420	382	1.10	0.0499	0.0011	0.2056	0.0045	0.0299	0.0004	190	27	190	4	190	3
HG01-56	155	170	0.91	0.0511	0.0010	0.2698	0.0056	0.0383	0.0005	246	25	243	4	242	3
HG01-57	162	243	0.67	0.0511	0.0012	0.2451	0.0059	0.0348	0.0005	245	31	223	5	220	3
HG01-58	228	450	0.51	0.0508	0.0008	0.2676	0.0042	0.0382	0.0005	233	17	241	3	242	3
HG01-60	302	508	0.59	0.0493	0.0010	0.1892	0.0038	0.0278	0.0004	162	24	176	3	177	2
HG01-59	99	71	1.39	0.0502	0.0023	0.2252	0.0100	0.0325	0.0006	204	70	206	8	206	4
HG01-61	1297	1401	0.93	0.0645	0.0007	1.1203	0.0139	0.1259	0.0015	759	12	763	7	764	9
HG01-62	264	290	0.91	0.0535	0.0013	0.3981	0.0094	0.0540	0.0007	351	29	340	7	339	5
HG01-63	784	1334	0.59	0.0510	0.0008	0.2105	0.0035	0.0300	0.0004	240	18	194	3	190	2
HG01-64	161	217	0.74	0.0504	0.0009	0.2750	0.0050	0.0396	0.0005	212	20	247	4	250	3
HG01-65	97	109	0.89	0.0519	0.0016	0.2927	0.0088	0.0409	0.0006	279	42	261	7	259	4
HG01-66	138	224	0.62	0.0508	0.0019	0.1948	0.0071	0.0278	0.0005	230	54	181	6	177	3
HG01-67	95	770	0.12	0.0554	0.0007	0.5237	0.0071	0.0686	0.0008	429	13	428	5	427	5
HG01-68	294	255	1.15	0.0506	0.0018	0.1770	0.0060	0.0254	0.0004	221	49	165	5	162	3
HG01-69	316	606	0.52	0.0501	0.0007	0.2612	0.0038	0.0378	0.0005	201	15	236	3	239	3
HG01-70	48	52	0.92	0.0513	0.0018	0.2776	0.0097	0.0393	0.0006	253	51	249	8	248	4
HG01-71	172	166	1.04	0.0514	0.0010	0.2824	0.0058	0.0399	0.0005	257	24	253	5	252	3
HG01-72	85	154	0.55	0.0503	0.0013	0.2408	0.0064	0.0348	0.0005	207	36	219	5	220	3
HG01-74	118	182	0.65	0.0498	0.0011	0.2010	0.0044	0.0293	0.0004	183	27	186	4	186	2
HG01-75	180	242	0.74	0.0504	0.0010	0.1814	0.0036	0.0261	0.0003	214	23	169	3	166	2
HG01-77	78	555	0.14	0.0504	0.0007	0.2701	0.0039	0.0389	0.0005	211	15	243	3	246	3
HG01-78	33	90	0.37	0.0505	0.0015	0.2346	0.0067	0.0337	0.0005	217	39	214	5	214	3
HG01-79	159	365	0.44	0.0488	0.0013	0.1767	0.0048	0.0263	0.0004	136	37	165	4	167	2
HG01-80	190	690	0.28	0.0515	0.0007	0.2733	0.0042	0.0385	0.0005	264	16	245	3	243	3

(*Continued*)

Table 1. *Continued*

Q14

Spots	Element (ppm)		Th/U	Corrected isotopic ratios						Corrected ages (Ma)					
	Th	U		$^{207}Pb/^{206}Pb$	1σ	$^{207}Pb/^{235}U$	1σ	$^{206}Pb/^{238}U$	1σ	$^{207}Pb/^{206}Pb$	1σ	$^{207}Pb/^{235}U$	1σ	$^{206}Pb/^{238}U$	1σ
HG01-81	163	269	0.61	0.0503	0.0010	0.2301	0.0045	0.0332	0.0004	211	23	210	4	210	3
HG01-83	245	285	0.86	0.0496	0.0008	0.2023	0.0034	0.0296	0.0004	174	19	187	3	188	2
HG01-84	660	680	0.97	0.0566	0.0007	0.5389	0.0074	0.0691	0.0008	476	14	438	5	431	5
HG01-76	294	198	1.49	0.0521	0.0009	0.3248	0.0060	0.0452	0.0006	288	21	286	5	285	4
HG01-73	82	95	0.86	0.0496	0.0015	0.1906	0.0055	0.0279	0.0004	174	41	177	5	177	3
HG01-82	66	79	0.84	0.0506	0.0014	0.2644	0.0074	0.0379	0.0005	224	39	238	6	240	3
HG01-85	251	484	0.52	0.0519	0.0008	0.3029	0.0048	0.0423	0.0005	283	17	269	4	267	3
HG01-86	90	102	0.88	0.0529	0.0019	0.3106	0.0106	0.0426	0.0007	324	49	275	8	269	4
HG01-87	146	195	0.75	0.0562	0.0009	0.5548	0.0092	0.0716	0.0009	460	17	448	6	446	5
HG01-88	21	35	0.61	0.0533	0.0023	0.3062	0.0128	0.0417	0.0007	342	63	271	10	263	5
HG01-89	192	243	0.79	0.0516	0.0008	0.2978	0.0050	0.0418	0.0005	270	18	265	4	264	3
HG01-90	172	235	0.73	0.0501	0.0009	0.2124	0.0040	0.0308	0.0004	200	21	196	3	195	3
HG01-91	84	121	0.69	0.0492	0.0022	0.1294	0.0055	0.0191	0.0003	157	67	124	5	122	2
HG01-93	92	183	0.50	0.0501	0.0010	0.1856	0.0037	0.0269	0.0004	200	24	173	3	171	2
HG01-95	155	170	0.91	0.0505	0.0010	0.2086	0.0044	0.0300	0.0004	218	25	192	4	190	3
HG01-96	193	209	0.92	0.0558	0.0008	0.5492	0.0086	0.0714	0.0009	445	16	444	6	444	5
HG01-92	195	1052	0.19	0.0509	0.0006	0.3004	0.0041	0.0428	0.0005	235	14	267	3	270	3
HG01-94	60	125	0.48	0.0504	0.0013	0.2372	0.0061	0.0341	0.0005	215	34	216	5	216	3
HG01-97	64	92	0.69	0.0514	0.0015	0.2925	0.0086	0.0412	0.0006	260	41	260	7	261	4
HG01-98	505	494	1.02	0.0493	0.0011	0.1734	0.0040	0.0255	0.0004	163	29	162	3	162	2
HG01-99	156	78	2.00	0.0497	0.0015	0.1913	0.0056	0.0279	0.0004	179	42	178	5	178	3
HG01-100	544	636	0.85	0.0510	0.0007	0.2635	0.0041	0.0375	0.0005	242	16	237	3	237	3
HG01-101	135	303	0.44	0.0498	0.0009	0.2015	0.0039	0.0293	0.0004	188	23	186	3	186	2
HG01-102	38	40	0.97	0.0521	0.0020	0.3519	0.0133	0.0490	0.0008	288	56	306	10	309	5
HG01-103	94	269	0.35	0.0559	0.0008	0.5555	0.0089	0.0721	0.0009	447	16	449	6	449	5
HG01-104	222	177	1.26	0.0515	0.0010	0.2819	0.0056	0.0397	0.0005	261	23	252	4	251	3
HG01-105	82	73	1.13	0.0508	0.0014	0.2569	0.0071	0.0367	0.0005	232	38	232	6	232	3
HG01-106	199	273	0.73	0.0499	0.0010	0.2048	0.0040	0.0298	0.0004	189	23	189	3	189	2
HG01-107	133	155	0.86	0.0495	0.0020	0.1637	0.0063	0.0240	0.0004	173	59	154	6	153	3
HG01-108	500	810	0.62	0.0517	0.0007	0.2769	0.0042	0.0389	0.0005	270	16	248	3	246	3

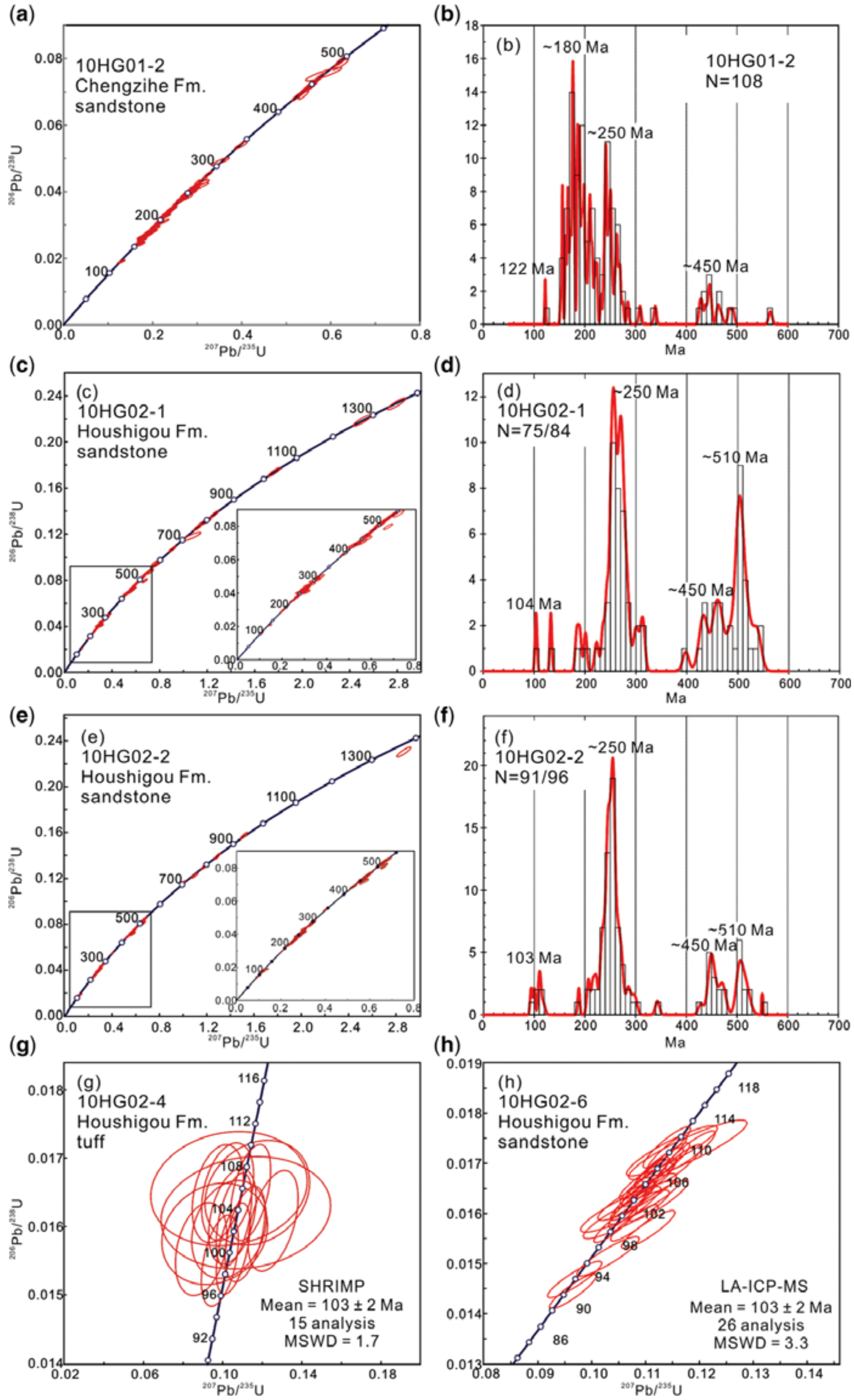

Fig. 8. (**a**) LA-ICP-MS U–Pb zircon Concordia diagram and (**b**) probability diagram of sandstone sample 10HG01-2 from the Chengzihe Formation. (**c**) LA-ICP-MS U–Pb zircon Concordia diagram and (**d**) probability diagram of sandstone sample 10HG02-1 from the Houshigou Formation. (**e**) LA-ICP-MS U–Pb zircon Concordia diagram and (**f**) probability diagram of sandstone sample 10HG02-2 from the Houshigou Formation. (**g**) SHRIMP zircon Concordia diagram for tuff sample 10HG02-4 from the Houshigou Formation. (**h**) LA-ICP-MS U–Pb Concordia diagram of sandstone sample 10HG02-6 from the Houshigou Formation. MSWD, mean standard weight of deviation.

Table 2. *LA-ICP-MS U–Pb results for detrital zircons from sample 10HG02-1, Houshigou Formation of the Hegang Basin*

Spots	Element (ppm)		Th/U	Corrected isotopic ratios						Corrected ages (Ma)					
	Th	U		$^{207}Pb/^{206}Pb$	1σ	$^{207}Pb/^{235}U$	1σ	$^{206}Pb/^{238}U$	1σ	$^{207}Pb/^{206}Pb$	1σ	$^{207}Pb/^{235}U$	1σ	$^{206}Pb/^{238}U$	1σ
HG2-1-01	72	308	0.23	0.0575	0.0010	0.6413	0.0123	0.0809	0.0012	511	20	503	8	501	7
HG2-1-02	303	715	0.42	0.0574	0.0012	0.6398	0.0139	0.0808	0.0012	507	24	502	9	501	7
HG2-1-03	112	170	0.66	0.0515	0.0021	0.2851	0.0114	0.0402	0.0007	263	58	255	9	254	5
HG2-1-04	267	718	0.37	0.0569	0.0009	0.6123	0.0112	0.0780	0.0011	488	19	485	7	484	7
HG2-1-05	203	367	0.55	0.0667	0.0011	1.2621	0.0225	0.1372	0.0020	829	17	829	10	829	11
HG2-1-06	230	292	0.79	0.0575	0.0016	0.5575	0.0152	0.0703	0.0011	512	33	450	10	438	7
HG2-1-07	232	367	0.63	0.0584	0.0013	0.5822	0.0135	0.0723	0.0011	544	26	466	9	450	7
HG2-1-08	238	308	0.77	0.0563	0.0014	0.5754	0.0146	0.0742	0.0012	463	30	461	9	461	7
HG2-1-09	397	403	0.99	0.0529	0.0014	0.2997	0.0082	0.0411	0.0007	323	34	266	6	260	4
HG2-1-10	103	253	0.41	0.0736	0.0013	1.7650	0.0340	0.1739	0.0025	1031	18	1033	12	1033	14
HG2-1-11	807	1154	0.70	0.0571	0.0010	0.6372	0.0120	0.0810	0.0012	494	19	501	7	502	7
HG2-1-12	303	271	1.12	0.0573	0.0011	0.6432	0.0136	0.0815	0.0012	502	23	504	8	505	7
HG2-1-13	152	377	0.40	0.0577	0.0010	0.6458	0.0124	0.0812	0.0012	516	20	506	8	504	7
HG2-1-14	265	352	0.75	0.0493	0.0015	0.1104	0.0033	0.0162	0.0003	162	42	106	3	104	2
HG2-1-15	109	239	0.46	0.0498	0.0011	0.2903	0.0068	0.0423	0.0006	183	29	259	5	267	4
HG2-1-16	95	168	0.56	0.0600	0.0013	0.7227	0.0159	0.0874	0.0013	602	24	552	9	540	8
HG2-1-17	120	255	0.47	0.0567	0.0010	0.6314	0.0122	0.0808	0.0011	479	21	497	8	501	7
HG2-1-18	210	478	0.44	0.0547	0.0012	0.3771	0.0087	0.0500	0.0007	400	27	325	6	314	4
HG2-1-19	198	225	0.88	0.0615	0.0011	0.6752	0.0131	0.0796	0.0011	656	20	524	8	494	7
HG2-1-20	124	1153	0.11	0.0569	0.0016	0.5735	0.0138	0.0731	0.0010	488	63	460	9	455	6
HG2-1-21	150	278	0.54	0.0533	0.0014	0.2983	0.0081	0.0406	0.0006	339	35	265	6	257	4
HG2-1-22	330	387	0.85	0.0566	0.0010	0.5870	0.0111	0.0752	0.0010	477	20	469	7	467	6
HG2-1-23	28	38	0.73	0.0657	0.0034	1.0666	0.0531	0.1177	0.0025	797	68	737	26	717	15
HG2-1-24	714	742	0.96	0.0518	0.0011	0.2946	0.0065	0.0412	0.0006	277	26	262	5	261	4
HG2-1-25	90	175	0.51	0.0553	0.0020	0.3090	0.0111	0.0405	0.0007	426	50	273	9	256	4
HG2-1-26	523	376	1.39	0.0522	0.0011	0.3090	0.0068	0.0429	0.0006	296	26	273	5	271	4
HG2-1-27	340	621	0.55	0.0523	0.0010	0.3125	0.0062	0.0433	0.0006	300	22	276	5	273	4
HG2-1-28	53	119	0.45	0.0515	0.0026	0.2916	0.0145	0.0411	0.0008	265	79	260	11	259	5
HG2-1-29	460	794	0.58	0.0511	0.0009	0.2702	0.0052	0.0384	0.0005	245	22	243	4	243	3
HG2-1-30	912	1545	0.59	0.0575	0.0009	0.6535	0.0110	0.0824	0.0011	512	17	511	7	510	7
HG2-1-31	284	447	0.64	0.0512	0.0010	0.2806	0.0059	0.0397	0.0006	250	24	251	5	251	3
HG2-1-32	117	182	0.65	0.0530	0.0024	0.2932	0.0127	0.0402	0.0007	327	65	261	10	254	5
HG2-1-33	701	1703	0.41	0.0514	0.0010	0.2820	0.0058	0.0398	0.0006	257	24	252	5	252	3
HG2-1-34	73	158	0.47	0.0614	0.0013	0.9072	0.0199	0.1071	0.0015	655	24	656	11	656	9

HG2-1-35	45	57	0.78	0.0656	0.0020	1.1795	0.0354	0.1304	0.0021	794	37	791	16	790	12
HG2-1-36	477	961	0.50	0.0519	0.0010	0.2663	0.0055	0.0372	0.0005	283	24	240	4	235	3
HG2-1-37	205	493	0.41	0.0519	0.0012	0.1493	0.0034	0.0209	0.0003	283	28	141	3	133	2
HG2-1-38	646	665	0.97	0.0500	0.0011	0.1996	0.0044	0.0290	0.0004	194	27	185	4	184	3
HG2-1-40	175	578	0.30	0.0514	0.0010	0.2994	0.0060	0.0423	0.0006	259	23	266	5	267	4
HG2-1-41	51	254	0.20	0.0595	0.0021	0.7613	0.0246	0.0929	0.0014	584	79	575	14	572	8
HG2-1-42	398	589	0.68	0.0576	0.0009	0.6585	0.0111	0.0829	0.0011	515	17	514	7	513	7
HG2-1-43	357	474	0.75	0.0511	0.0009	0.2869	0.0055	0.0408	0.0006	244	21	256	4	257	4
HG2-1-44	153	257	0.60	0.0524	0.0012	0.3121	0.0073	0.0432	0.0006	302	28	276	6	273	4
HG2-1-45	151	321	0.47	0.0573	0.0011	0.6393	0.0128	0.0809	0.0012	504	21	502	8	501	7
HG2-1-46	246	296	0.83	0.0517	0.0012	0.3036	0.0075	0.0426	0.0006	270	31	269	6	269	4
HG2-1-47	179	196	0.92	0.0502	0.0015	0.2194	0.0066	0.0317	0.0005	202	41	201	5	201	3
HG2-1-48	181	351	0.51	0.0519	0.0015	0.3213	0.0096	0.0449	0.0007	282	40	283	7	283	5
HG2-1-39	210	234	0.89	0.0576	0.0013	0.6632	0.0155	0.0835	0.0013	514	26	517	9	517	8
HG2-1-49	44	66	0.66	0.0831	0.0016	2.5095	0.0522	0.2190	0.0034	1273	19	1275	15	1276	18
HG2-1-50	32	70	0.46	0.0524	0.0025	0.3452	0.0159	0.0478	0.0009	301	70	301	12	301	6
HG2-1-51	170	270	0.63	0.0565	0.0012	0.5857	0.0137	0.0753	0.0012	471	26	468	9	468	7
HG2-1-52	466	1550	0.30	0.0575	0.0008	0.6472	0.0111	0.0817	0.0012	509	17	507	7	506	7
HG2-1-53	107	258	0.41	0.0527	0.0011	0.3604	0.0081	0.0497	0.0008	314	26	313	6	312	5
HG2-1-54	106	194	0.54	0.0518	0.0022	0.3071	0.0128	0.0430	0.0008	278	62	272	10	271	5
HG2-1-55	233	338	0.69	0.0520	0.0011	0.3216	0.0072	0.0449	0.0007	285	26	283	6	283	4
HG2-1-57	423	1061	0.40	0.0583	0.0009	0.7017	0.0126	0.0874	0.0013	540	18	540	8	540	7
HG2-1-58	146	323	0.45	0.0869	0.0014	2.7942	0.0506	0.2331	0.0034	1359	16	1354	14	1351	18
HG2-1-56	52	85	0.62	0.0554	0.0023	0.5233	0.0214	0.0685	0.0013	430	58	427	14	427	8
HG2-1-59	125	208	0.60	0.0516	0.0013	0.3026	0.0079	0.0426	0.0007	267	33	268	6	269	4
HG2-1-60	339	179	1.90	0.0539	0.0021	0.3546	0.0133	0.0477	0.0008	368	53	308	10	300	5
HG2-1-61	181	272	0.66	0.0517	0.0012	0.3103	0.0077	0.0435	0.0007	273	30	274	6	275	4
HG2-1-62	350	780	0.45	0.0576	0.0009	0.6620	0.0113	0.0833	0.0012	515	17	516	7	516	7
HG2-1-63	160	262	0.61	0.0518	0.0012	0.3158	0.0078	0.0442	0.0007	278	31	279	6	279	4
HG2-1-64	23	490	0.05	0.0546	0.0012	0.4793	0.0113	0.0637	0.0010	396	27	398	8	398	6
HG2-1-65	240	619	0.39	0.0580	0.0011	0.7556	0.0153	0.0946	0.0014	528	21	571	9	583	8
HG2-1-66	274	353	0.78	0.0507	0.0016	0.2463	0.0079	0.0353	0.0006	225	44	224	6	223	4
HG2-1-67	291	405	0.72	0.0578	0.0010	0.6728	0.0127	0.0845	0.0012	521	20	522	8	523	7
HG2-1-68	258	340	0.76	0.0513	0.0014	0.2859	0.0079	0.0404	0.0006	256	36	255	6	255	4
HG2-1-69	133	353	0.38	0.0647	0.0012	1.1201	0.0221	0.1257	0.0018	763	20	763	11	763	10
HG2-1-70	123	215	0.57	0.0556	0.0015	0.5328	0.0147	0.0696	0.0011	434	34	434	10	434	7
HG2-1-72	117	162	0.72	0.0554	0.0017	0.5263	0.0164	0.0690	0.0011	427	41	429	11	430	7
HG2-1-71	463	680	0.68	0.0514	0.0011	0.2877	0.0063	0.0406	0.0006	257	25	257	5	257	4

(Continued)

Table 2. *Continued*

Spots	Element (ppm)		Th/U	Corrected isotopic ratios						Corrected ages (Ma)					
	Th	U		$^{207}Pb/^{206}Pb$	1σ	$^{207}Pb/^{235}U$	1σ	$^{206}Pb/^{238}U$	1σ	$^{207}Pb/^{206}Pb$	1σ	$^{207}Pb/^{235}U$	1σ	$^{206}Pb/^{238}U$	1σ
HG2-1-73	557	553	1.01	0.0499	0.0012	0.2057	0.0051	0.0299	0.0004	192	32	190	4	190	3
HG2-1-74	152	203	0.75	0.0510	0.0016	0.2687	0.0083	0.0382	0.0006	243	43	242	7	242	4
HG2-1-75	169	435	0.39	0.0580	0.0011	0.6870	0.0135	0.0860	0.0012	529	21	531	8	532	7
HG2-1-76	336	690	0.49	0.0568	0.0010	0.6078	0.0115	0.0777	0.0011	483	20	482	7	482	7
HG2-1-77	194	249	0.78	0.0518	0.0014	0.3117	0.0083	0.0437	0.0007	276	34	275	6	275	4
HG2-1-78	58	76	0.77	0.0514	0.0037	0.2912	0.0202	0.0411	0.0010	259	116	260	16	260	6
HG2-1-79	93	83	1.12	0.0481	0.0067	0.1097	0.0149	0.0166	0.0006	104	233	106	14	106	4
HG2-1-80	384	261	1.47	0.0513	0.0014	0.2777	0.0078	0.0393	0.0006	253	37	249	6	248	4
HG2-1-81	243	240	1.01	0.0562	0.0014	0.5715	0.0149	0.0738	0.0011	460	32	459	10	459	7
HG2-1-82	97	133	0.73	0.0520	0.0021	0.3012	0.0119	0.0421	0.0007	283	59	267	9	266	4
HG2-1-83	241	598	0.40	0.0573	0.0010	0.6426	0.0124	0.0813	0.0011	504	20	504	8	504	7
HG2-1-84	51	63	0.81	0.0522	0.0030	0.3224	0.0180	0.0448	0.0009	294	90	284	14	283	6

Sample 10HG02-2

Sample 10HG02-2 was also collected from the Houshigou Formation. Zircon grains were 40–200 μm long and a total of 96 randomly selected grains were analysed (Table 3); all grains were concordant at the 90% confidence level. The $^{206}Pb/^{238}U$ ages mainly fall into three populations (Fig. 8e): 286–207 Ma (60%), 475–429 Ma (14%) and 524–502 Ma (10%), with peaks at approximately 250, 450 and 510 Ma, respectively (Fig. 8f), identical to the populations in sample 10HG02-1. The youngest zircon has a $^{206}Pb/^{238}U$ age of 94 ± 2 Ma. However, sample 10HG02-2 cannot be younger than sample 10HG02-4 according to the field relationships. Since there is only one grain younger than 100 Ma, the mean age of 103 ± 2 Ma given by five Cretaceous zircons probably represents the best estimate of the age of the stratum. There are also six Precambrian zircons with $^{207}Pb/^{206}Pb$ ages ranging from 1.4 to 0.7 Ga.

Sample 10HG02-4

Sample 10HG02-4 was collected from the tuff layer in the upper part of Houshigou Formation, stratigraphically above samples 10HG02-1 and 10HG02-2. Zircon grains were mostly 70 μm long, with 2:1 aspect ratios. Seventeen zircon grains were analysed by SHRIMP (Table 4). The measured U and Th concentrations varied from 195 to 1119 ppm and from 89 to 645 ppm, respectively. The Th/U ratio ranges from 0.40 to 0.66. One grain was excluded from the calculation because it is considered to be an inherited zircon with an age of 256 ± 7 Ma. The remaining 16 analyses give a weighted mean age of 103 ± 2 Ma (mean square weighted deviation (MSWD) = 1.7) (Fig. 8g), recording the eruption time of the tuff. This is coeval, within error, of the best estimate of the age of deposition of the underlying Houshigou Formation, suggesting rapid deposition within the Hegang Basin.

Sample 10HG02-6

This sample was collected from a sandstone unit above the tuff layer in the upper part of the Houshigou Formation. Zircon grains were mostly 70 μm long, with 2:1 aspect ratios. Thirty-six zircon grains were analysed using LA-ICP-MS (Table 5), and the U and Th concentrations varied from 111 to 1330 ppm and from 83 to 1240 ppm, respectively, with Th/U ratios ranging from 0.52 to 1.72. Twenty-six analyses (excluding five discordant grains and five inherited grains with ages of 117, 185, 208, 270 and 516 Ma) give a weighted mean age of 103 ± 2 Ma (MSWD = 3.3) (Fig. 8h), suggesting that most of the zircons were derived either from the tuff or from strata immediately underlying the tuff.

Discussion

Detrital zircon provenance change in the Hegang Basin

According to the data presented above, both the Chengzihe and Houshigou formations have provenance sources from terranes characterized by ages of around 250 and 450 Ma. However, the Chengzihe Formation is dominated by approximately 180 Ma zircons, whereas the Houshigou Formation has no Late Triassic–Early Jurassic zircons but, instead, has zircons of around 510 Ma.

The approximately 250, 450 and 510 Ma provenance was most probably derived from the Jiamusi Block to the east, which consists of both Late Permian granites and Pan-African granites and gneiss (Wilde *et al.* 1997; Zhou *et al.* 2009, 2010, 2011*a*; W u*et al.* 2011).

The provenance of 180 Ma was possibly from the LXR to the west, since this is a dominant age in this region (Wu *et al.* 2011). The LXR consists dominantly of Early Jurassic bimodal igneous rocks related to intraplate extension triggered by subduction (Wu *et al.* 2011; Yang *et al.* 2012; Yu *et al.* 2012) and some Palaeozoic igneous rocks (Meng *et al.* 2011; Wang *et al.* 2012*a*, *b*). The age distribution map (Fig. 9) shows that approximately 210–170 Ma magmatism is not present in the Jiamusi Block, and is mainly distributed in the LXR and ZR (to the west of the Mudanjiang Fault) on the eastern margin of the Songliao Block.

Hence, the Hegang Basin had two main provenances: the LXR and the Jiamusi Block. At about 122 Ma, the Hegang Basin received sediments from both of these sources; however, at around 103 Ma, when the Houshigou Formation was deposited, the LXR source was no longer available. Considering the seismic structure of the Hegang Basin and the fact that the Chengzihe, Muling and Dongshan formations thicken eastwards with westwards onlap on to the basement, whereas the Houshigou Formation has no change in thickness, we propose that the Hegang Basin was separated from the Songliao Basin by the LXR when the Chengzihe, Muling and Dongshan formations were deposited but was connected to the Songliao Basin across the LXR when the Houshigou Formation was deposited at some time between 122 and 103 Ma.

Connection to the Songliao Basin

If the Hegang Basin was eventually connected with the Songliao Basin in Aptian–Albian time, the latter

Table 3. *LA-ICP-MS U–Pb results for detrital zircons from sample 10HG02-2, Houshigou Formation of the Hegang Basin*

Spots	Element (ppm)		Th/U	Corrected isotopic ratios						Corrected ages (Ma)					
	Th	U		$^{207}Pb/^{206}Pb$	1σ	$^{207}Pb/^{235}U$	1σ	$^{206}Pb/^{238}U$	1σ	$^{207}Pb/^{206}Pb$	1σ	$^{207}Pb/^{235}U$	1σ	$^{206}Pb/^{238}U$	1σ
HG02-01	263	700	0.38	0.0510	0.0009	0.2852	0.0050	0.0406	0.0005	241	19	255	4	256	3
HG02-02	270	325	0.83	0.0514	0.0010	0.2722	0.0055	0.0384	0.0005	259	24	244	4	243	3
HG02-03	461	556	0.83	0.0517	0.0008	0.2808	0.0045	0.0394	0.0005	273	17	251	4	249	3
HG02-04	66	300	0.22	0.0532	0.0008	0.4010	0.0067	0.0547	0.0007	336	18	342	5	343	4
HG02-05	268	385	0.69	0.0517	0.0009	0.3075	0.0055	0.0431	0.0006	273	20	272	4	272	3
HG02-06	677	1158	0.58	0.0595	0.0008	0.6642	0.0100	0.0809	0.0010	587	15	517	6	502	6
HG02-07	292	546	0.53	0.0510	0.0009	0.2645	0.0050	0.0376	0.0005	240	22	238	4	238	3
HG02-09	163	193	0.85	0.0511	0.0011	0.2735	0.0059	0.0388	0.0005	245	26	245	5	246	3
HG02-10	124	836	0.15	0.0532	0.0009	0.3315	0.0060	0.0452	0.0006	336	20	291	5	285	4
HG02-11	320	186	1.72	0.0495	0.0028	0.1192	0.0064	0.0175	0.0004	173	88	114	6	112	2
HG02-08	120	111	1.08	0.0509	0.0017	0.3046	0.0097	0.0434	0.0007	238	46	270	8	274	4
HG02-12	177	261	0.68	0.0516	0.0010	0.2998	0.0059	0.0421	0.0006	269	23	266	5	266	3
HG02-13	1048	1132	0.93	0.0537	0.0008	0.2862	0.0043	0.0386	0.0005	360	16	256	3	244	3
HG02-14	340	531	0.64	0.0565	0.0007	0.5925	0.0079	0.0761	0.0009	472	13	472	5	473	6
HG02-15	270	357	0.76	0.0554	0.0011	0.5259	0.0109	0.0688	0.0009	430	24	429	7	429	5
HG02-16	91	141	0.65	0.0511	0.0022	0.2772	0.0115	0.0393	0.0007	246	63	248	9	249	4
HG02-17	234	335	0.70	0.0565	0.0007	0.5847	0.0082	0.0751	0.0009	471	14	467	5	467	6
HG02-18	165	225	0.73	0.0559	0.0010	0.5544	0.0100	0.0719	0.0009	450	19	448	7	448	6
HG02-19	105	402	0.26	0.0649	0.0011	1.0973	0.0197	0.1226	0.0016	771	18	752	10	746	9
HG02-20	186	333	0.56	0.0515	0.0010	0.2967	0.0058	0.0418	0.0005	264	23	264	5	264	3
HG02-23	360	569	0.63	0.0672	0.0008	1.2906	0.0167	0.1393	0.0017	845	12	842	7	840	10
HG02-22	267	616	0.43	0.0515	0.0007	0.2915	0.0042	0.0411	0.0005	262	15	260	3	260	3
HG02-21	187	158	1.18	0.0656	0.0009	1.1793	0.0174	0.1303	0.0016	795	14	791	8	790	9
HG02-24	268	391	0.69	0.0513	0.0009	0.2877	0.0054	0.0407	0.0005	256	21	257	4	257	3
HG02-25	249	438	0.57	0.0511	0.0007	0.2833	0.0043	0.0402	0.0005	245	16	253	3	254	3
HG02-26	430	319	1.35	0.0514	0.0010	0.2836	0.0056	0.0400	0.0005	258	23	254	4	253	3
HG02-27	180	309	0.58	0.0500	0.0018	0.1172	0.0041	0.0170	0.0003	196	52	113	4	109	2
HG02-28	332	280	1.18	0.0495	0.0009	0.2228	0.0040	0.0327	0.0004	170	21	204	3	207	3
HG02-29	274	571	0.48	0.0508	0.0007	0.2710	0.0040	0.0387	0.0005	232	15	243	3	245	3
HG02-30	264	484	0.54	0.0514	0.0011	0.2484	0.0054	0.0351	0.0005	257	27	225	4	222	3
HG02-31	637	1233	0.52	0.0699	0.0008	1.5151	0.0192	0.1572	0.0019	926	12	936	8	941	11
HG02-32	215	259	0.83	0.0572	0.0013	0.5690	0.0129	0.0722	0.0010	499	27	457	8	449	6
HG02-33	195	315	0.62	0.0513	0.0008	0.2872	0.0049	0.0406	0.0005	256	19	256	4	256	3
HG02-34	81	94	0.86	0.0503	0.0018	0.2264	0.0080	0.0327	0.0005	208	53	207	7	207	3
HG02-35	54	311	0.17	0.0520	0.0018	0.2893	0.0096	0.0403	0.0006	287	48	258	8	255	4
HG02-36	302	399	0.76	0.0513	0.0010	0.2862	0.0056	0.0404	0.0005	256	23	256	4	256	3
HG02-37	182	291	0.63	0.0514	0.0008	0.2860	0.0049	0.0403	0.0005	260	19	255	4	255	3

HG02-39	212	301	0.71	0.0576	0.0007	0.6677	0.0095	0.0841	0.0010	515	14	519	6	520	6
HG02-40	122	89	1.37	0.0480	0.0033	0.0967	0.0065	0.0146	0.0003	98	105	94	6	94	2
HG02-41	235	538	0.44	0.0517	0.0010	0.2720	0.0055	0.0381	0.0005	273	24	244	4	241	3
HG02-42	843	986	0.85	0.0515	0.0009	0.2735	0.0047	0.0385	0.0005	262	19	246	4	244	3
HG02-43	476	711	0.67	0.0525	0.0010	0.2814	0.0053	0.0389	0.0005	305	21	252	4	246	3
HG02-44	644	950	0.68	0.0535	0.0009	0.2873	0.0049	0.0389	0.0005	351	18	256	4	246	3
HG02-45	186	553	0.34	0.0525	0.0011	0.2474	0.0054	0.0342	0.0005	305	27	224	4	217	3
HG02-46	241	951	0.25	0.0520	0.0017	0.2671	0.0079	0.0373	0.0005	285	76	240	6	236	3
HG02-47	653	847	0.77	0.0499	0.0008	0.2039	0.0034	0.0297	0.0004	188	18	188	3	188	2
HG02-48	313	552	0.57	0.0514	0.0008	0.2942	0.0046	0.0415	0.0005	257	16	262	4	262	3
HG02-38	116	186	0.63	0.0574	0.0010	0.6465	0.0112	0.0817	0.0011	508	18	506	7	506	6
HG02-49	71	82	0.88	0.0527	0.0024	0.2956	0.0129	0.0407	0.0007	317	66	263	10	257	5
HG02-50	356	650	0.55	0.0513	0.0008	0.2809	0.0046	0.0397	0.0005	256	18	251	4	251	3
HG02-52	252	326	0.77	0.0531	0.0008	0.2902	0.0045	0.0396	0.0005	333	16	259	4	251	3
HG02-53	250	587	0.43	0.0571	0.0007	0.6377	0.0087	0.0810	0.0010	495	13	501	5	502	6
HG02-54	66	112	0.59	0.0519	0.0017	0.2695	0.0084	0.0377	0.0006	281	44	242	7	238	4
HG02-55	293	329	0.89	0.0515	0.0012	0.2861	0.0069	0.0403	0.0006	263	31	255	5	255	3
HG02-56	78	102	0.77	0.0572	0.0011	0.6459	0.0124	0.0819	0.0011	498	21	506	8	508	6
HG02-57	254	484	0.52	0.0535	0.0007	0.2919	0.0044	0.0396	0.0005	349	15	260	3	250	3
HG02-59	148	344	0.43	0.0560	0.0010	0.5634	0.0107	0.0729	0.0010	454	21	454	7	454	6
HG02-60	663	772	0.86	0.0520	0.0011	0.2684	0.0058	0.0375	0.0005	284	26	241	5	237	3
HG02-58	280	1236	0.23	0.0627	0.0007	1.0020	0.0133	0.1160	0.0014	697	13	705	7	707	8
HG02-51	62	320	0.19	0.0568	0.0011	0.5985	0.0114	0.0765	0.0010	483	21	476	7	475	6
HG02-61	84	205	0.41	0.0581	0.0014	0.5740	0.0137	0.0717	0.0010	533	29	461	9	446	6
HG02-62	128	391	0.33	0.0523	0.0013	0.2537	0.0061	0.0352	0.0005	300	31	230	5	223	3
HG02-63	232	402	0.58	0.0526	0.0010	0.2640	0.0053	0.0364	0.0005	310	23	238	4	231	3
HG02-64	187	155	1.20	0.0480	0.0022	0.1037	0.0046	0.0157	0.0003	100	69	100	4	100	2
HG02-65	56	159	0.35	0.0565	0.0012	0.5875	0.0126	0.0754	0.0010	473	25	469	8	469	6
HG02-66	172	337	0.51	0.0513	0.0009	0.2823	0.0052	0.0399	0.0005	253	21	253	4	252	3
HG02-67	328	759	0.43	0.0525	0.0008	0.2667	0.0042	0.0368	0.0005	309	16	240	3	233	3
HG02-68	215	261	0.83	0.0569	0.0010	0.5766	0.0105	0.0735	0.0010	489	20	462	7	457	6
HG02-69	252	708	0.36	0.0571	0.0007	0.6464	0.0090	0.0821	0.0010	495	14	506	6	509	6
HG02-70	145	874	0.17	0.0577	0.0006	0.6644	0.0085	0.0836	0.0010	517	13	517	5	517	6
HG02-71	107	149	0.72	0.0518	0.0012	0.2896	0.0067	0.0406	0.0006	276	29	258	5	256	3
HG02-72	148	328	0.45	0.0517	0.0008	0.3061	0.0052	0.0429	0.0005	273	19	271	4	271	3
HG02-73	384	631	0.61	0.0575	0.0007	0.6569	0.0090	0.0829	0.0010	511	13	513	5	513	6
HG02-74	274	397	0.69	0.0511	0.0008	0.2736	0.0044	0.0388	0.0005	245	17	246	3	246	3
HG02-75	144	123	1.17	0.0524	0.0014	0.3435	0.0093	0.0476	0.0007	301	36	300	7	300	4
HG02-76	87	104	0.83	0.0560	0.0011	0.5625	0.0110	0.0729	0.0010	450	22	453	7	454	6
HG02-77	93	312	0.30	0.0504	0.0011	0.2356	0.0051	0.0339	0.0005	213	27	215	4	215	3
HG02-78	242	262	0.92	0.0571	0.0008	0.5663	0.0089	0.0720	0.0009	495	16	456	6	448	5

(*Continued*)

Table 3. *Continued*

Spots	Element (ppm)		Th/U	Corrected isotopic ratios						Corrected ages (Ma)					
	Th	U		$^{207}Pb/^{206}Pb$	1σ	$^{207}Pb/^{235}U$	1σ	$^{206}Pb/^{238}U$	1σ	$^{207}Pb/^{206}Pb$	1σ	$^{207}Pb/^{235}U$	1σ	$^{206}Pb/^{238}U$	1σ
HG02-79	502	561	0.89	0.0512	0.0008	0.2763	0.0047	0.0392	0.0005	248	18	248	4	248	3
HG02-80	93	456	0.20	0.0514	0.0008	0.2871	0.0046	0.0405	0.0005	257	17	256	4	256	3
HG02-81	52	134	0.39	0.0514	0.0012	0.2899	0.0067	0.0410	0.0006	257	29	258	5	259	3
HG02-82	232	426	0.54	0.0512	0.0008	0.2793	0.0048	0.0396	0.0005	248	19	250	4	250	3
HG02-83	34	76	0.44	0.0579	0.0013	0.6751	0.0147	0.0846	0.0012	525	25	524	9	524	7
HG02-84	198	201	0.98	0.0517	0.0009	0.3110	0.0059	0.0436	0.0006	273	21	275	5	275	4
HG02-85	539	713	0.75	0.0514	0.0007	0.2925	0.0043	0.0413	0.0005	259	15	261	3	261	3
HG02-86	190	198	0.96	0.0529	0.0015	0.3312	0.0090	0.0454	0.0007	326	36	291	7	286	4
HG02-87	157	219	0.71	0.0903	0.0011	2.8671	0.0391	0.2303	0.0029	1431	12	1373	10	1336	15
HG02-88	255	366	0.70	0.0592	0.0008	0.6648	0.0101	0.0814	0.0010	576	15	518	6	504	6
HG02-89	22	29	0.74	0.0491	0.0052	0.1245	0.0128	0.0184	0.0006	155	173	119	12	117	4
HG02-90	193	472	0.41	0.0527	0.0011	0.2659	0.0055	0.0366	0.0005	314	24	239	4	232	3
HG02-91	205	527	0.39	0.0514	0.0010	0.2717	0.0054	0.0383	0.0005	259	23	244	4	243	3
HG02-94	112	236	0.47	0.0568	0.0009	0.5637	0.0091	0.0720	0.0009	485	16	454	6	448	6
HG02-95	278	293	0.95	0.0539	0.0010	0.3025	0.0058	0.0407	0.0005	367	21	268	4	257	3
HG02-96	119	295	0.40	0.0530	0.0014	0.3408	0.0091	0.0466	0.0007	331	35	298	7	294	4
HG02-92	1181	763	1.55	0.0525	0.0008	0.3060	0.0050	0.0422	0.0005	309	17	271	4	267	3
HG02-93	300	611	0.49	0.0517	0.0007	0.3015	0.0046	0.0423	0.0005	271	16	268	4	267	3

Table 4. *SHRIMP U–Pb results for zircons from tuff sample 10HG02-4, Houshigou Formation of the Hegang Basin*

Sample No.	Th (ppm)	U (ppm)	Th/U	^{206}Pb (ppm)	^{206}Pb (%)	$^{204}Pb^*/^{206}Pb^*$	±%	$^{207}Pb^*/^{206}Pb^*$	±%	$^{207}Pb^*/^{235}U$	±%	$^{206}Pb^*/^{238}U$	±%	Error	% Discordant	$^{207}Pb/^{235}U$ Age (Ma)	$^{207}Pb/^{235}U$ 1σ	$^{206}Pb/^{238}U$ Age (Ma)	$^{206}Pb/^{238}U$ 1σ
HG02401	141	353	0.40	12.5	1.52	0.0008	24	0.0503	6.6	0.2815	7.2	0.0406	2.9	0.40	1.8	252	16	256	7
HG02402	614	1119	0.55	15.7	1.13	0.0006	22	0.0476	4.8	0.1057	5.6	0.0161	2.8	0.50	1.1	102	5	103	3
HG02403	324	666	0.49	9.1	1.49	0.0008	29	0.0412	9.2	0.0891	9.6	0.0157	2.9	0.30	15.8	87	8	100	3
HG02404	212	329	0.64	4.7	1.62	0.0009	55	0.0516	14.5	0.1175	14.9	0.0165	3.1	0.21	6.4	113	16	106	3
HG02405	89	195	0.46	2.9	4.10	0.0022	32	0.0452	25.1	0.1032	25.3	0.0166	3.3	0.13	6.3	100	24	106	4
HG02406	165	422	0.39	5.9	1.88	0.0010	33	0.0469	11.7	0.1032	12.1	0.0160	3.0	0.25	2.5	100	12	102	3
HG02407	497	1022	0.49	13.9	0.77	0.0004	30	0.0487	4.6	0.1053	5.4	0.0157	2.8	0.53	1.3	102	5	100	3
HG02408	319	754	0.42	10.6	0.92	0.0005	33	0.0470	7.0	0.1049	7.5	0.0162	2.9	0.38	2.1	101	7	103	3
HG02409	339	684	0.50	8.5	1.32	0.0007	24	0.0461	6.6	0.0911	7.2	0.0143	2.9	0.40	3.6	89	6	92	3
HG02410	185	295	0.63	4.2	2.97	0.0016	29	0.0438	18.1	0.0960	18.4	0.0159	3.1	0.17	9.3	93	16	102	3
HG02411	485	887	0.55	11.9	0.93	0.0005	30	0.0461	5.6	0.0986	6.3	0.0155	2.8	0.46	4.0	96	6	99	3
HG02412	413	848	0.49	11.7	0.91	0.0005	32	0.0507	5.2	0.1113	6.0	0.0159	2.9	0.49	5.0	107	6	102	3
HG02413	223	544	0.41	7.6	1.00	0.0005	36	0.0565	5.9	0.1255	6.6	0.0161	3.0	0.46	14.2	120	8	103	3
HG02414	338	862	0.39	12.4	1.41	0.0008	29	0.0450	8.0	0.1025	8.5	0.0165	2.9	0.34	6.7	99	8	106	3
HG02415	269	641	0.42	9.2	1.48	0.0008	27	0.0429	8.3	0.0976	8.8	0.0165	2.9	0.33	11.5	95	8	106	3
HG02416	645	1115	0.58	15.9	0.84	0.0005	35	0.0501	5.2	0.1140	5.9	0.0165	2.8	0.48	3.6	110	6	106	3
HG02417	150	249	0.60	3.6	4.19	0.0023	34	0.0499	25.1	0.1117	25.3	0.0162	3.3	0.13	3.5	108	26	104	3

Errors are 1-sigma; Pb* indicates the radiogenic portions. Common lead correction was based on measured ^{204}Pb.

Table 5. *LA-ICP-MS U–Pb results for detrital zircons from sample 10HG02-6, Houshigou Formation of the Hegang Basin*

Spots	Element (ppm)		Th/U	Corrected isotopic ratios						Corrected ages (Ma)					
	Th	U		$^{207}Pb/^{206}Pb$	1σ	$^{207}Pb/^{235}U$	1σ	$^{206}Pb/^{238}U$	1σ	$^{207}Pb/^{206}Pb$	1σ	$^{207}Pb/^{235}U$	1σ	$^{206}Pb/^{238}U$	1σ
HG2-6-001	196	133	1.48	0.0497	0.0025	0.1394	0.0069	0.0204	0.0004	182	79	133	6	130	3
HG2-6-003	337	526	0.64	0.0495	0.0013	0.1079	0.0029	0.0158	0.0002	173	36	104	3	101	2
HG2-6-004	726	855	0.85	0.0485	0.0012	0.1138	0.0029	0.0170	0.0003	125	33	109	3	109	2
HG2-6-005	765	962	0.80	0.0498	0.0013	0.1183	0.0030	0.0173	0.0003	184	33	114	3	110	2
HG2-6-006	537	786	0.68	0.0480	0.0010	0.1092	0.0024	0.0165	0.0002	100	26	105	2	105	2
HG2-6-007	765	1131	0.68	0.0481	0.0010	0.1139	0.0025	0.0172	0.0003	103	26	110	2	110	2
HG2-6-008	620	775	0.80	0.0480	0.0011	0.1080	0.0025	0.0163	0.0002	101	29	104	2	104	2
HG2-6-009	274	430	0.64	0.0479	0.0017	0.0968	0.0033	0.0147	0.0002	92	50	94	3	94	2
HG2-6-010	83	111	0.75	0.0495	0.0031	0.1179	0.0073	0.0173	0.0004	172	99	113	7	110	2
HG2-6-011	426	574	0.74	0.0480	0.0015	0.1105	0.0035	0.0167	0.0003	101	45	106	3	107	2
HG2-6-012	198	331	0.60	0.0525	0.0013	0.3093	0.0078	0.0428	0.0007	307	31	274	6	270	4
HG2-6-002	605	665	0.91	0.0511	0.0015	0.1105	0.0033	0.0157	0.0003	246	39	106	3	100	2
HG2-6-013	603	682	0.89	0.0477	0.0012	0.1140	0.0029	0.0173	0.0003	84	32	110	3	111	2
HG2-6-014	822	1127	0.73	0.0479	0.0010	0.1107	0.0024	0.0167	0.0003	96	26	107	2	107	2
HG2-6-015	1240	1330	0.93	0.0481	0.0010	0.1066	0.0023	0.0161	0.0002	102	25	103	2	103	2
HG2-6-017	770	865	0.89	0.0496	0.0012	0.1161	0.0029	0.0170	0.0003	174	32	112	3	109	2
HG2-6-018	484	691	0.70	0.0500	0.0017	0.1267	0.0044	0.0184	0.0003	195	48	121	4	117	2
HG2-6-019	351	532	0.66	0.0482	0.0014	0.1102	0.0033	0.0166	0.0003	108	40	106	3	106	2
HG2-6-020	397	586	0.68	0.0575	0.0010	0.6618	0.0123	0.0834	0.0012	512	19	516	7	516	7
HG2-6-021	595	751	0.79	0.0480	0.0012	0.1076	0.0027	0.0162	0.0003	101	32	104	3	104	2
HG2-6-022	276	429	0.64	0.0574	0.0020	0.1391	0.0048	0.0176	0.0003	506	45	132	4	112	2
HG2-6-023	829	886	0.94	0.0482	0.0013	0.1125	0.0030	0.0169	0.0003	110	34	108	3	108	2
HG2-6-024	272	434	0.63	0.0501	0.0017	0.1123	0.0037	0.0163	0.0003	200	46	108	3	104	2
HG2-6-016	210	298	0.71	0.0482	0.0022	0.1084	0.0048	0.0163	0.0003	107	67	105	4	104	2
HG2-6-025	1155	1278	0.90	0.0485	0.0014	0.0965	0.0029	0.0144	0.0002	122	41	94	3	92	1
HG2-6-026	215	218	0.98	0.0483	0.0025	0.1064	0.0053	0.0160	0.0003	114	76	103	5	102	2
HG2-6-027	811	936	0.87	0.0494	0.0019	0.1030	0.0038	0.0151	0.0003	165	55	100	4	97	2
HG2-6-028	43	69	0.62	0.0482	0.0047	0.1091	0.0104	0.0164	0.0005	109	158	105	9	105	3
HG2-6-029	314	226	1.39	0.0505	0.0014	0.2281	0.0064	0.0328	0.0005	216	37	209	5	208	3
HG2-6-030	783	993	0.79	0.0485	0.0014	0.1081	0.0031	0.0162	0.0003	124	40	104	3	103	2
HG2-6-031	123	148	0.83	0.0481	0.0037	0.1042	0.0077	0.0157	0.0004	104	117	101	7	100	3
HG2-6-032	636	814	0.78	0.0480	0.0012	0.1044	0.0027	0.0158	0.0002	99	33	101	2	101	2
HG2-6-033	256	489	0.52	0.0498	0.0014	0.1997	0.0056	0.0291	0.0005	184	37	185	5	185	3
HG2-6-035	113	159	0.72	0.0483	0.0024	0.1149	0.0056	0.0173	0.0003	114	75	110	5	110	2
HG2-6-036	62	116	0.54	0.0507	0.0063	0.1056	0.0125	0.0151	0.0006	226	194	102	11	97	4
HG2-6-034	260	150	1.73	0.0481	0.0028	0.1070	0.0060	0.0161	0.0003	103	86	103	5	103	2

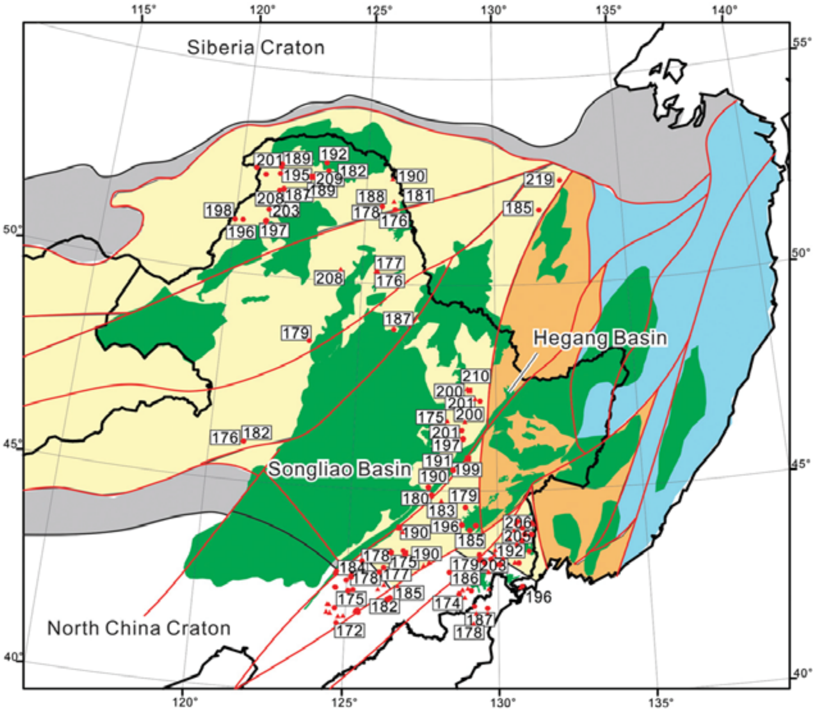

Fig. 9. Map of NE China and adjacent areas showing the igneous rock distribution (*c.* 210–170 Ma) and highlighting that the Jiamusi Block has no Late Triassic–Early Jurassic magmatism. Data are from Wu *et al.* (2011), Yang *et al.* (2012) and Yu *et al.* (2012).

should also record the same change in provenance in the late Early Cretaceous.

The tuff at the top of the Houshigou Formation has an age of 103 ± 2 Ma, whereas the youngest age group from the Chengzihe Formation has a peak age of 122 ± 2 Ma. It appears likely that the Chengzihe, Muling and Dongshan formations in the Hegang Basin correspond to the Shahezi, Yingcheng and Denglouku formations, respectively, in the Songliao Basin (Feng *et al.* 2010*a*, *b*; Li *et al.* 2012). Also, the Houshigou Formation in the Hegang Basin corresponds to the Quantou Formation of the Songliao basin (Zhao *et al.* 2013) (Fig. 10).

The Denglouku Formation in the Songliao Basin contains approximately 180 Ma detrital zircons that were most probably also derived from the LXR, further suggesting that the LXR was a highland and the two basins were not connected at this time. However, there is no evidence of such an Early Jurassic provenance in the Quantou Formation in the Songliao Basin (Fig. 11), indicating that the LXR was not an existing barrier at this time, and that the Songliao Basin was connected to the Hegang Basin across the LXR when the Yaojia Formation in the Songliao Basin and Houshigou Formation in the Hegang Basin were deposited. It is important to note that the Quantou Formation in the Songliao Basin has 1.8 Ga provenance zircons (most probably derived from the North China Craton), whereas the Houshigou Formation in the Hegang Basin does not contain these. This is possibly because the connection between the Hegang and Songliao basins was restricted. The Lesser Xing'an Range was probably still an uplift area beneath the water and this blocked detritus from the North China Craton into the Hegang Basin. This could explain why only the Songliao Basin contains 1.8 Ga zircons of North China Craton provenance.

The early Late Cretaceous Yaojia Formation in the Songliao Basin also contains no Early Jurassic zircons (Fig. 11), suggesting that the Songliao Basin possibly flooded over the LXR during the whole of its post-rift stage from the Quantou Formation to the Yaojia Formation, as per the subdivision suggested by Feng *et al.* (2010*a*). This leaves the question of when were the Songliao and Hegang basins again separated by the LXR as occurs at the present time? Li *et al.* (2012) indicated that the fourth member (as shown in Fig. 10) of the Nenjiang Formation in the Songliao Basin does contain an early Jurassic provenance (Fig. 11), so the second separation of the Hegang and Songliao basins must have occurred at the time when the fourth member of the Nenjiang formation was deposited. Importantly, this also marks the beginning of the structural inversion of the Songliao Basin (Feng *et al.* 2010*a*, *b*).

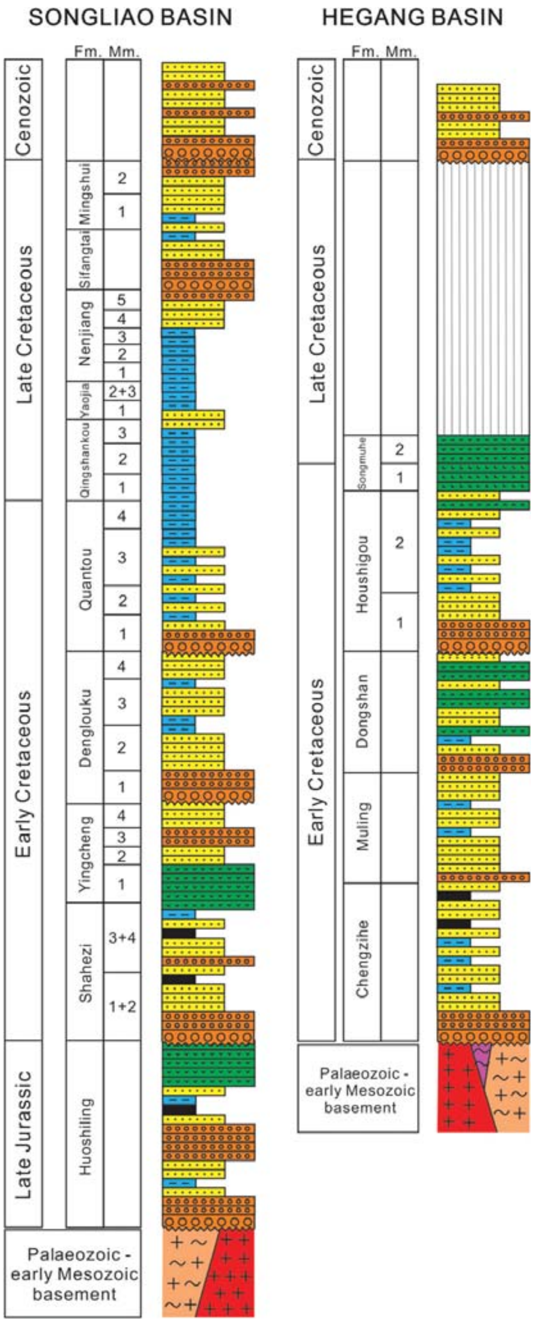

Fig. 10. Stratigraphy of the Songliao and Hegang basins. The column for the Songliao Basin follows Feng *et al.* (2010*a*); the column for the Hegang Basin is based on the Hegang and Jiamusi 1:200 000 geological maps.

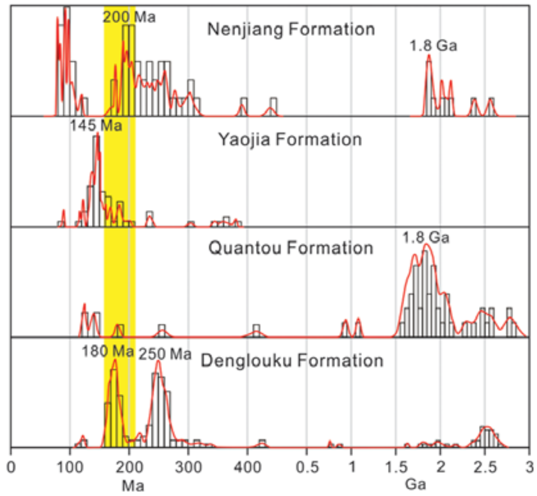

Fig. 11. Detrital zircon data for the Denglouku, Quantou, Yaojia and Nenjiang formations of the Songliao Basin. Data are from Li *et al.* (2012) and Zhao *et al.* (2013).

Depositional model and tectonic implications

In summary, the Songliao and Hegang basins formed a unified system in the Cretaceous. We identify four stages that illustrate the evolution of the Songliao and Hegang basin system (see Fig. 12a): synrift, post-rift, inversion and present day, following the model developed for the Songliao Basin (Feng *et al.* 2010*a*). In the synrift stage, the LXR was a highland. The Songliao and Hegang basins received sediments from the LXR during the Barremian–Early Albian, resulting in deposition of the Denglouku Formation in the Songliao Basin, and the Chengzihe, Muling and Dongshan formations in the Hegang Basin. In the post-rift stage, the LXR was under water and unable to provide detritus to the evolving basins. The Songliao and Hegang basins were then connected, and this led to the deposition of the Quantou, Qingshankou, Yaojia and Nenjiang formations in the Songliao Basin, and the Houshigou Formation in the Hegang Basin. In the inversion stage, the eastern part of the Songliao Block and the Jiamusi Block were uplifted, and the LXR, again, provided detritus to the Songliao Basin, while there was no deposition in the Hegang Basin. At the present time, the LXR is being eroded and separates the Songliao Basin from the Hegang Basin.

The schematic depositional model (Fig. 12a) best explains the provenance change and indicates a process of eastwards migration of the depositional centre of the Songliao and Hegang basin system, and also a lateral reverse event after the extension. However, greater consideration of the tectonic implications is needed.

Considering the direction of the migration and regional tectonic background, this process was most possibly triggered by the palaeo-Pacific Ocean to the east rather than subduction of the

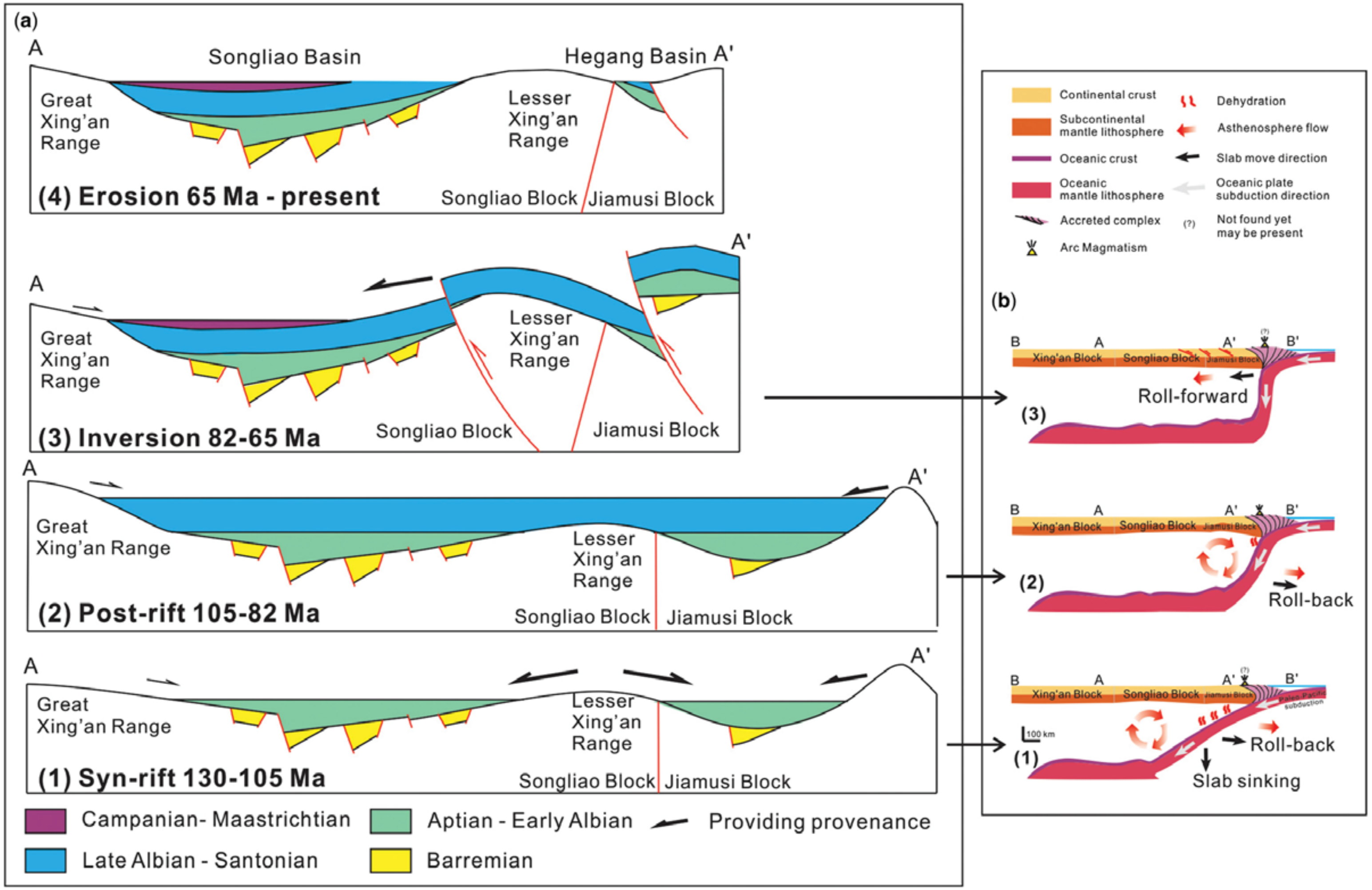

Fig. 12. (**a**) Depositional model showing the evolution of the Songliao–Hegang basin system: (1) synrift, (2) post-rift, (3) inversion and (4) erosion, based on the model for the Songliao Basin (Feng *et al.* 2010*a*). (**b**) Tectonic model showing Palaeo-Pacific subduction, and slab roll-back and roll-forward (after Sun *et al.* 2013).

Mongol–Okhotsk Ocean to the north, as the Mongol–Okhotsk Ocean was closed in the Early Cretaceous (Cogne *et al.* 2005), whereas the events recorded in this study mainly occurred in the mid-Cretaceous. Slab roll-back and roll-forward are two major models controlling the geological evolution of continental margins affected by oceanic subduction (Schellart *et al.* 2008). Thus, a tectonic model with a sequence of slab roll-back and roll-forward for the palaeo-Pacific subduction is built as shown in Figure 12b to interpret the evolution of the Hegang and Songliao basins.

The evolution of the subduction model is divided into three stages as shown in Figure 12b (1) In the first stage, the slab subducted to the mantle beneath the Songliao Basin. The mantle convection area and the extensional centre were also beneath/at the Songliao Basin. (2) In the second stage, the slab rolled back and the subducting slab angle increased, triggered by slab sinking. The mantle convection area and the extensional centre migrated eastwards beneath the Hegang Basin, causing the eastwards migration of the depositional centre and the connection between the Hegang and Songliao basins. (3) In the third stage, the slab subducting angle increased to nearly vertical, and the slab sinking could no longer trigger slab roll-back or an increase in the slab angle, so extension stopped instead of resulting in a regional uplift and thrust event.

The above tectonic model not only satisfies the sedimentary evolution of the Hegang and Songliao basins but is also consistent with a previous model postulated according to the magmatic evolution of NE China at this time (Sun *et al.* 2013).

Conclusions

Our new detrital zircon data from the Chengzihe and Houshigou formations in the Hegang Basin, combined with our SHRIMP data from a tuff at the top of the Houshigou Formation, allow us to evaluate the provenance of detritus entering the Hegang Basin and to also place a precise timeline on the age of the Houshigou Formation. When these data are combined with the seismic structure of the Hegang Basin, an evaluation of the stratigraphy in both the Hegang and Songliao basins, an evaluation of previously published detrital zircon data for the Songliao Basin and an overview of the regional tectonic setting, we are able to make the following conclusions:

- The Hegang Basin is a Cretaceous coal-bearing clastic sedimentary basin in which the Chengzihe, Muling and Dongshan formations thicken eastwards with westwards onlap on to the LXR, whereas the Houshigou Formation shows no change in thickness.
- The SHRIMP zircon age of a tuff from the upper part of the Houshigou Formation in the Hegang Basin is 103 ± 2 Ma, implying that the Houshigou Formation is equivalent to the Quantou Formation in the Songliao Basin.
- The Chengzihe Formation of the Hegang Basin and the Denglouku Formation of the Songliao Basin show striking similarities in their detrital zircon provenance, with approximately 180 Ma zircons indicating that the Lesser Xing'an Range was possibly a highland at this time and able to provide detritus to the evolving basins.
- The Houshigou Formation of the Hegang Basin and the Quantou Formation of the Songliao Basin both lack zircons with ages of around 180 Ma, which suggests that the Lesser Xing'an Range was possibly under water and unable to provide detritus during the post-rift stage.
- The Songliao and Hegang basins show an eastwards migration of the deposition centre of the Cretaceous basin system in NE China. This implies lithospheric extension and, when taken in a regional context, this was most probably driven by palaeo-Pacific roll-back.

We appreciate the assistance of B. Wu and D.-X. Chen during LA-ICP-MS analysis. H.-Q. Xie and G.-H. Gong helped with the SHRIMP analysis. We also thank C.-W. Dong, X.-Q. Zhao, Y. Xu, J. Xiao, L.-M. Tang and X. Yu for help in the field and with sample pretreatment. Thanks to G. Gibson, W. Xiao and an anonymous reviewer for their significant contribution to the final quality of the manuscript. This work was supported by the National Science and Technology Major Project (grant No. 2011ZX05009-001), the National Natural Science Foundation of China (grant No. 41272231, 41330207) and the Zhejiang Provincial Natural Science Foundation of China (grant No. Y5100131). It is TIGeR (The Institute for Geoscience Research) paper No. 483.

References

Andersen, T. 2002. Correction of common lead in U–Pb analyses that do not report Pb-204. *Chemical Geology*, **192**, 59–79.

Black, L. P. & Gulson, B. L. 1978. The age of the Mud Tank carbonatite, Strangways Range, Northern Territory. *BMR Journal of Australian Geology and Geophysics*, **3**, 227–232.

Black, L. P., Kamo, S. L., Allen, C. M., Aleinikoff, J. N., Davis, D. W., Korsch, R. J. & Foudoulis, C. 2003. TEMORA 1: a new zircon standard for Phanerozoic U–Pb geochronology. *Chemical Geology*, **200**, 155–170.

Cawood, P. A., Nemchin, A. A., Freeman, M. & Sircombe, K. 2003. Linking source and sedimentary basin: detrital zircon record of sediment flux along a modern river system and implications for provenance studies. *Earth and Planetary Science Letters*, **210**, 259–268.

Cawood, P. A., Hawkesworth, C. J. & Dhuime, B. 2012. Detrital zircon record and tectonic setting. *Geology*, **40**, 875–878.

Cogne, J. P., Kravchinsky, V. A., Halim, N. & Hankard, F. 2005. Late Jurassic–Early Cretaceous closure of the Mongol-Okhotsk Ocean demonstrated by new Mesozoic palaeomagnetic results from the Trans-Baikal area (SE Siberia). *Geophysical Journal International*, **163**, 813–832.

Dickinson, W. R. & Gehrels, G. E. 2009. Use of U–Pb ages of detrital zircons to infer maximum depositional ages of strata: a test against a Colorado Plateau Mesozoic database. *Earth and Planetary Science Letters*, **288**, 115–125.

Drewery, S., Cliff, R. A. & Leeder, M. R. 1987. Provenance of carboniferous sandstones from U–Pb dating of detrital zircons. *Nature*, **325**, 50–53.

Feng, Z. Q., Jia, C. Z., Xie, X. N., Zhang, S., Feng, Z. H. & Cross, T. A. 2010*a*. Tectonostratigraphic units and stratigraphic sequences of the nonmarine Songliao basin, northeast China. *Basin Research*, **22**, 79–95.

Feng, Z. Q., Zhang, S. *et al.* 2010*b*. Lacustrine turbidite channels and fans in the Mesozoic Songliao Basin, China. *Basin Research*, **22**, 96–107.

Feng, Z. H., Fang, W. *et al.* 2011. Depositional environment of terrestrial petroleum source rocks and geochemical indicators in the Songliao Basin. *Science China Earth Sciences*, **54**, 1304–1317.

Feng, Z., Wang, C., Graham, S., Koeberl, C., Dong, H., Huang, Y. & Gao, Y. 2013. Continental scientific drilling project of cretaceous Songliao basin: scientific objectives and drilling technology. *In*: Wang, C., Graham, S. A., Parrish, J. T. & Wan, X. (eds) *Environmental/Climate Change in the Cretaceous Greenhouse World: Records from Terrestrial Scientific Drilling of Songliao Basin and Adjacent Area of China. Palaeogeography, Palaeoclimatology, Palaeoecology*, **385**, 6–16.

Gao, F. H., Xu, W. L., Yang, D. B., Pei, F. P., Liu, X. M. & Hu, Z. C. 2007. LA-ICP-MS zircon U–Pb dating from granitoids in southern basement of Songliao basin: constraints on ages of the basin basement. *Science in China Series D*, **50**, 995–1004.

Gao, Y. F., Wang, P. J., Qu, X. J. & Wang, G. D. 2010. Sedimentary facies and cyclostratigraphy of the Cretaceous first member of Nenjiang Formation in the Southeast uplift zone, Songliao Basin and its correlation with the CCSD-SK-I. *Acta Petrologica Sinica*, **26**, 99–108.

Gu, Z. W., Li, Z. S. & Yu, X. H. 1997. *Lower Cretaceous Bivalves from the Eastern Heilongjiang Province of China*. Science Press, Beijing.

Huang, Q. H., Yang, J. G. & Kong, H. 2003. The Fangzheng Formation of the Fangzheng Rift in the Northeast of the Yilan–Yitong Rift Valley and its significance. *Journal of Stratigraphy*, **27**, 138–145. [in Chinese with English abstract].

Jackson, M. & Sherman, G. D. 1953. Chemical weathering of minerals in soils. *Advances in Agronomy*, **5**, 317.

Jackson, S. E., Pearson, N. J., Griffin, W. L. & Belousova, E. A. 2004. The application of laser ablation-inductively coupled plasma-mass spectrometry to *in situ* U–Pb zircon geochronology. *Chemical Geology*, **211**, 47–69.

Kotov, A. B., Velikoslavinskii, S. D. *et al.* 2009. Age of the Amur Group of the Bureya-Jiamusi Superterrane in the Central Asian Fold Belt: Sm–Nd Isotope evidence. *Doklady Earth Sciences*, **429**, 1245–1248.

Kravchinsky, V. A., Cogne, J. P., Harbert, W. P. & Kuzmin, M. I. 2002. Evolution of the Mongol–Okhotsk Ocean as constrained by new palaeomagnetic data from the Mongol–Okhotsk suture zone, Siberia. *Geophysical Journal International*, **148**, 34–57.

Li, S.-Q., Chen, F., Siebel, W., Wu, J.-D., Zhu, X.-Y., Shan, X.-L. & Sun, X.-M. 2012. Late Mesozoic tectonic evolution of the Songliao basin, NE China: evidence from detrital zircon ages and Sr–Nd isotopes. *Gondwana Research*, **22**, 943–955.

Li, Y. C., Yang, X. P., Zhou, X. F. & Wang, H. J. 2006. Integrated stratigraphic correlation of the Jixi Group and Longzhaogou Group in eastern Heilongjiang China. *Geology in China*, **33**, 1312–1320. [in Chinese with English abstract].

Li, Z. X., Zhang, L. H. & Powell, C. M. 1995. South China in Rodinia – part of the missing link between Australia East Antarctica and Laurentia. *Geology*, **23**, 407–410.

Liu, F. X. 2006. *Bennettitales from Lower Cretaceous Chengzihe Formation in the Jixi basin of Heilongjiang, China*. PhD thesis, Jilin University, 6–8.

Ludwig, K. R. 2001. *Squid 1.03: A User's Manual*. Berkeley Geochronology Center, Special Publications, **2**. Berkeley, CA.

Ludwig, K. R. 2003. *User's Manual for Isoplot 3.0. A Geochronological Toolkit for Microsoft Excel*. Berkeley Geochronology Center, Special Publications, **4**. Berkeley, CA.

Meng, E., Xu, W. L., Pei, F. P., Yang, D. B., Yu, Y. & Zhang, X. Z. 2010. Detrital-zircon geochronology of Late Paleozoic sedimentary rocks in eastern Heilongjiang Province, NE China: implications for the tectonic evolution of the eastern segment of the Central Asian Orogenic Belt. *Tectonophysics*, **485**, 42–51.

Meng, E., Xu, W. L., Pei, F. P., Yang, D. B., Wang, F. & Zhang, X. Z. 2011. Permian bimodal volcanism in the Zhangguangcai Range of eastern Heilongjiang Province, NE China: zircon U–Pb–Hf isotopes and geochemical evidence. *Journal of Asian Earth Sciences*, **41**, 119–132.

Pei, F. P., Xu, W. L., Yang, D. B., Zhao, Q. G., Liu, X. M. & Hu, Z. C. 2007. Zircon U–Pb geochronology of basement metamorphic rocks in the Songliao Basin. *Chinese Science Bulletin*, **52**, 942–948.

Ren, J. Y., Tamaki, K., Li, S. T. & Junxia, Z. 2002. Late Mesozoic and Cenozoic rifting and its dynamic setting in Eastern China and adjacent areas. *Tectonophysics*, **344**, 175–205.

Riggs, N. R., Lehman, T. M., Gehrels, G. E. & Dickinson, W. R. 1996. Detrital zircon link between headwaters and terminus of the upper Triassic Chinle–Dockum paleoriver system. *Science*, **273**, 97–100.

Schellart, W. P., Stegman, D. R. & Freeman, J. 2008. Global trench migration velocities and slab migration induced upper mantle volume fluxes: constraints to find an Earth reference frame based on minimizing viscous dissipation. *Earth-Science Reviews*, **88**, 118–144.

Sha, J. G. 2007. Cretaceous stratigraphy of northeast China: non-marine and marine correlation. *Cretaceous Research*, **28**, 146–170.

Sha, J. G., Cai, H. W. *et al.* 2002. Studies on the Early Cretaceous Longzhaogou and Jixi Groups of eastern Heilongjiang, northeast China, and their bearing on the age of supposedly Jurassic strata in eastern Asia. *Journal of Asian Earth Sciences*, **20**, 141–150.

Sha, J. G., Matsukawa, M., Cai, H. W., Jiang, B. Y., Ito, M., He, C. Q. & Gu, Z. W. 2003. The upper Jurassic–Lower Cretaceous of eastern Heilongjiang, Northeast China: stratigraphy and regional basin history. *Cretaceous Research*, **24**, 715–728.

Sha, J. G., Wang, J. P. *et al.* 2009. Upper Jurassic and lower cretaceous of Sanjiang-Middle Amur basin: non-marine and marine correlation. *Science in China Series D*, **52**, 1873–1889.

Sorokin, A. A., Kotov, A. B., Sal'nikova, E. B., Kudryashov, N. M., Anisimova, I. V., Yakovleva, S. Z. & Fedoseenko, A. M. 2010. Granitoids of the Tyrma–Bureya complex in the northern Bureya–Jiamusi superterrane of the Central Asian fold belt: age and geodynamic setting. *Russian Geology and Geophysics*, **51**, 563–571.

Sun, G. & Dilcher, D. L. 2002. Early angiosperms from the Lower Cretaceous of Jixi, eastern Heilongjiang, China. *Review of Palaeobotany and Palynology*, **121**, 91–112.

Sun, M. D., Chen, H. L., Zhang, F. Q., Wilde, S. A., Dong, C. W. & Yang, S. F. 2013. A 100 Ma bimodal composite dyke complex in the Jiamusi Block, NE China: an indication for lithospheric extension driven by Paleo-Pacific roll-back. *Lithos*, **162**, 317–330.

Sun, X. M., Long, S. X., Zhang, M. S., Liu, X. Y. & Hao, F. J. 2006. Discovery and timing of major thrustbelt in Jiamusi-Yitong fault zone. *Oil and Gas Geology*, **27**, 637–643. [in Chinese with English abstract].

Thomas, W. A. 2011. Detrital-zircon geochronology and sedimentary provenance. *Lithosphere*, **3**, 304–308.

Wan, Y. S., Li, R. W. *et al.* 2005. UHP metamorphism and exhumation of the Dabie Orogen, China: evidence from SHRIMP dating of zircon and monazite from a UHP granitic gneiss cobble from the Hefei Basin. *Geochimica et Cosmochimica Acta*, **69**, 4333–4348.

Wang, C., Feng, Z., Zhang, L., Huang, Y., Cao, K., Wang, P. & Zhao, B. 2013. Cretaceous paleogeography and paleoclimate and the setting of SKI borehole sites in Songliao Basin, northeast China. *In*: Wang, C., Graham, S. A., Parrish, J. T. & Wan, X. (eds) *Environmental/Climate Change in the Cretaceous Greenhouse World: Records from Terrestrial Scientific Drilling of Songliao Basin and Adjacent Area of China. Palaeogeography, Palaeoclimatology, Palaeoecology*, **385**, 17–30.

Wang, C. W., Li, N., Sun, Y. W. & Zong, P. 2011. Distribution of Tuvaella brachiopod fauna and its tectonic significance. *Journal of Earth Sciences*, **22**, 11–19.

Wang, F., Xu, W. L., Gao, F. H., Meng, E., Cao, H. H., Zhao, L. & Yang, Y. 2012*a*. Tectonic history of the Zhangguangcailing Group in eastern Heilongjiang Province, NE China: constraints from U–Pb geochronology of detrital and magmatic zircons. *Tectonophysics*, **566**, 105–122.

Wang, F., Xu, W. L., Meng, E., Cao, H. H. & Gao, F. H. 2012*b*. Early Paleozoic amalgamation of the Songmen-Zhangguangcai Range and Jiamusi massifs in the eastern segment of the Central Asian Orogenic Belt: geochronological and geochemical evidence from granitoids and rhyolites. *Journal of Asian Earth Sciences*, **49**, 234–248.

Wang, Y., Zhang, F. Q. *et al.* 2006. Zircon SHRIMP U–Pb dating of meta-diorite from the basement of the Songliao Basin and its geological significance. *Chinese Science Bulletin*, **51**, 1877–1883.

Wilde, S. A., Dorsett-Bain, H. L. & Lennon, R. G. 1999. Geological setting and controls on the development of graphite, sillimanite and phosphate mineralization within the Jiamusi Massif: an exotic fragment of Gondwanaland located in north-eastern China? *Gondwana Research*, **2**, 21–46.

Wilde, S. A., Zhang, X. Z. & Wu, F. Y. 2000. Extension of a newly identified 500 Ma metamorphic terrane in North East China: further U–Pb SHRIMP dating of the Mashan Complex, Heilongjiang Province, China. *Tectonophysics*, **328**, 115–130.

Wilde, S. A., Wu, F. Y. & Zhang, X. Z. 2003. Late Pan-African magmatism in northeastern China: SHRIMP U–Pb zircon evidence from granitoids in the Jiamusi Massif. *Precambrian Research*, **122**, 311–327.

Wu, F. Y., Sun, D. Y., Li, H. M. & Wang, X. L. 2000. Zircon U–Pb ages of the basement rocks beneath the Songliao Basin, NE China. *Chinese Science Bulletin*, **45**, 1514–1518.

Wu, F. Y., Sun, D. Y., Li, H. M. & Wang, X. L. 2001. The nature of basement beneath the Songliao Basin in NE China: geochemical and isotopic constraints. *Physical Chemistry of Earth Part A*, **26**, 793–803.

Wu, F. Y., Yang, J. H., Lo, C. H., Wilde, S. A., Sun, D. Y. & Jahn, B. M. 2007*a*. The Heilongjiang Group: a Jurassic accretionary complex in the Jiamusi Massif at the western Pacific margin of northeastern China. *Island Arc*, **16**, 156–172.

Wu, F. Y., Sun, D. Y., Ge, W. C., Zhang, Y. B., Grant, M. L., Wilde, S. A. & Jahn, B. M. 2011. Geochronology of the Phanerozoic granitoids in northeastern China. *Journal of Asian Earth Sciences*, **41**, 1–30.

Wu, G., Sun, F. Y., Zhao, C. S., Li, Z. T., Zhao, A. L., Pang, Q. B. & Li, G. Y. 2005. Discovery of the Early Paleozoic post-collisional granites in northern margin of the Erguna massif and its geological significance. *Chinese Science Bulletin*, **50**, 2733–2743.

Wu, H. Y., Liang, X. D., Xiang, C. F. & Wang, Y. W. 2007*b*. Characteristics of petroleum accumulation in syncline of the Songliao basin and discussion on its accumulation mechanism. *Science in China Series D*, **50**, 702–709.

Xi, D. P., Wan, X. Q. *et al.* 2011. Discovery of Late Cretaceous foraminifera in the Songliao Basin: evidence from SK-1 and implications for identifying seawater incursions. *Chinese Science Bulletin*, **56**, 253–256.

Xiao, W., Windley, B. F., Hao, J. & Zhai, M. 2003. Accretion leading to collision and the Permian Solonker suture, Inner Mongolia, China: termination of the central Asian orogenic belt. *Tectonics*, **22**, 1069, http://dx.doi.org/10.1029/2002TC001484

Xiao, W., Mao, Q. *et al.* 2010. Paleozoic multiple accretionary and collisional processes of the Beishan orogenic collage. *American Journal of Science*, **310**, 1553–1594.

Xiao, W. J., Kroner, A. & Windley, B. 2009. Geodynamic evolution of Central Asia in the Paleozoic and Mesozoic. *International Journal of Earth Sciences*, **98**, 1185–1188.

Yang, Y. C., Han, S. J., Sun, D. Y., Guo, J. & Zhang, S. J. 2012. Geological and geochemical features and geochronology of porphyry molybdenum deposits in the Lesser Xing' an Range-Zhangguangcai Range metallogenic belt. *Acta Petrologica Sinica*, **28**, 379–390.

Yu, J. J., Wang, F., Xu, W. L., Gao, F. H. & Pei, F. P. 2012. Early Jurassic mafic magmatism in the Lesser Xing'an-Zhangguangcai Range, NE China, and its tectonic implications: constraints from zircon U–Pb chronology and geochemistry. *Lithos*, **142**, 256–266.

Yu, X., Xiao, J., Chen, H. L., Zhang, F. Q., Xu, Y., Dong, C. W. & Pang, Y. M. 2008. Phanerozoic magmatic events in the basement of Songliao basin: SHRIMP dating of captured zircons from Yingcheng Formation volcanic rocks. *Acta Petrologica Sinica*, **24**, 1123–1130.

Zhang, F. Q., Chen, H. L. *et al.* 2012. Late Mesozoic–Cenozoic evolution of the Sanjiang Basin in NE China and its tectonic implications for the West Pacific continental margin. *In*: Xiao, W., Li, S., Santosh, M. & Jahn, B. (eds) *Orogenic Belts in Central Asia: Correlations and Connections*. *Journal of Asian Earth Sciences*, **49**, 287–299.

Zhang, Y. Y. & Bao, L. N. 2009. Cretaceous Phytoplankton Assemblages from Songke Core-1, North and South (SK-1, N and S) of Songliao Basin, Northeast China. *Acta Geologica Sinica – English*, **83**, 868–874.

Zhao, B., Wang, C., Wang, X. & Feng, Z. 2013. Late Cretaceous (Campanian) provenance change in the Songliao Basin, NE China: evidence from detrital zircon U–Pb ages from the Yaojia and Nenjiang Formations. *In*: Wang, C., Graham, S. A., Parrish, J. T. & Wan, X. (eds) *Environmental/Climate Change in the Cretaceous Greenhouse World: Records from Terrestrial Scientific Drilling of Songliao Basin and Adjacent Area of China. Palaeogeography, Palaeoclimatology, Palaeoecology*, **385**, 83–94.

Zhou, J. B., Wilde, S. A., Zhang, X. Z., Zhao, G. C., Zheng, C. Q., Wang, Y. J. & Zhang, X. H. 2009. The onset of Pacific margin accretion in NE China: evidence from the Heilongjiang high-pressure metamorphic belt. *Tectonophysics*, **478**, 230–246.

Zhou, J. B., Wilde, S. A., Zhao, G. C., Zhang, X. Z., Wang, H. & Zeng, W. S. 2010. Was the easternmost segment of the Central Asian orogenic belt derived from Gondwana or Siberia: an intriguing dilemma? *Journal of Geodynamics*, **50**, 300–317.

Zhou, J. B., Wilde, S. A. *et al.* 2011*a*. A > 1300 km late Pan-African metamorphic belt in NE China: new evidence from the Xing'an block and its tectonic implications. *Tectonophysics*, **509**, 280–292.

Zhou, J. B., Zhang, X. Z., Wilde, S . A . & Zheng, C . Q . 2011*b*. Confirming of the Heilongjiang similar to 500 Ma Pan-African khondalite belt and its tectonic implications. *Acta Petrologica Sinica*, **27**, 1235–1245.

Zhou, J. B., Wilde, S. A., Zhang, X. Z., Liu, F. L. & Liu, J. H. 2012. Detrital zircons from Phanerozoic rocks of the Songliao Block, NE China: evidence and tectonic implications. *Journal of Asian Earth Sciences*, **47**, 21–34.